PCCP

# Melting of a single ice microparticle on exposure to focused near-IR laser beam to yield a supercooled water droplet


| | |
|---|---|
| Journal: | *Physical Chemistry Chemical Physics* |
| Manuscript ID | CP-ART-11-2023-005306.R1 |
| Article Type: | Paper |
| Date Submitted by the Author: | 12-Dec-2023 |
| Complete List of Authors: | Hashimoto, Shuichi; National Institute of Technology Gunma College, Advanced Engineering course<br>UWADA, Takayuki; Josai University, Department of Chemistry |
| | |

PCCP
Physical Chemistry Chemical Physics

# Guidelines for Reviewers

Thank you very much for your agreeing to review this manuscript for *Physical Chemistry Chemical Physics (PCCP)*.

*PCCP* is an international journal for the publication of cutting-edge original work in physical chemistry, chemical physics and biophysical chemistry, spanning experiment, theory, computation and data science. To be suitable for publication in *PCCP*, articles must include significant innovation and/or insight into physical chemistry; this is the most important criterion that reviewers and the Editors will judge against when evaluating submissions. Further information on our scope can be found at rsc.li/pccp.

*PCCP's* Impact Factor is **3.945** (2021 Journal Citation Reports®)

*The following manuscript has been submitted for consideration as a*

## *PAPER*

Full papers should contain original scientific work that has not been published previously. Full papers based on Communications are encouraged provided that they represent a substantial extension of the original material. There are no restrictions on the length of a paper. Authors should include a brief discussion in the Introduction that sets the context for the new work and gives their motivation for carrying out the study.

When preparing your report, please:

- Focus on the originality, importance, impact and reliability of the science. English language and grammatical errors do not need to be discussed in detail, except where it impedes scientific understanding.
- Use the journal scope and expectations to assess the manuscript's suitability for publication in *PCCP*.
- State clearly whether you think the article should be accepted or rejected and include details of how the science presented in the article corresponds to publication criteria.
- Inform the Editor if there is a conflict of interest, a significant part of the work you cannot review with confidence or if parts of the work have previously been published.

Best regards,

**Professor Anouk Rijs**
Editorial Board Chair
Vrije Universiteit Amsterdam, The Netherlands

**Dr Michael A. Rowan**
Executive Editor
Royal Society of Chemistry

Contact us

Please visit our reviewer hub for further details of our processes, policies and reviewer responsibilities as well as guidance on how to review, or click the links below.

What to do when you review

Reviewer responsibilities

Process & policies

point by point response to the referees' comments

---

Reviewers' report(s):

Referee: 1

---

**[Comments to the Author]**

The paper at hand reports on a carefully performed experimental study on the melting of ice microparticles stimulated by near IR radiation. The particles were supported on a glass substrate and the transition between the solid and the liquid state was detected by infrared Raman spectroscopy and optical images.

For me the central scientific aspect of this work is the following: Free water droplets of the size examined here are thermodynamically unstable at ambient temperature, they completely evaporate on a second or below second time scale. This dynamics is reduced at lower temperatures but heating by radiation can easily produce local temperatures high enough to stimulate evaporation. Sublimation wins over melting. This was the most probable interpretation of a previous study. In the present work ice-liquid and liquid-ice transitions of particles are unambiguously shown by IR Raman spectroscopy, supported by optical images. The transitions occur in the regime of supercooled water, this means between a stable (ice) and a metastable phase state (liquid). Further the temperature distribution in the droplet was numerically simulated with the COMSOL software package and used to interpret the experiments.

For me the general experimental finding of this work is a clear and interesting result. However, I see critical open issues with regard to the interpretation.

---

**[Author reply]**

I know that big labor is needed to go through the MS in a limited time. I really appreciate the referee for taking time to read our MS very carefully. I am glad to know that the referee finds our result interesting. I will explain below issues raised by the referee.

---

**[Comments to the Author]**

1) To illustrate the significance of this work the authors refer to a seminal paper by Richardson and coworkers who observed upon heating sublimation instead of melting of ice particles. They achieved the energy transfer by heating of gold nanoaggregates instead of IR overtone excitation in the present study. It is stated that millimeter sized particles are heated by heating gold aggregates. So it is not a bulk experiment and I am still puzzled as to why the one experiments shows melting and the other one does not. For larger aggregates and bulk the evaporation speed is lower because of the vanishing Kelvin effect. Evaporation should be less effective. For me the local barriers to ice

nucleation and melting are critical. The means that interactions with substrate surfaces on the outside and dopants in the inside are important.

Did you try other surfaces? Was there a particle-surface contact in the work of Richardson and coworkers? The simulated temperature profiles assume a homogeneous and isotropic situation and cannot resolve the effect of active sites that support melting and freezing. In a comprehensive paper on nanoscale water phase transitions (Moberg et al., PNAS 116, 2019, 24413) the different surface structures of ice-like and liquid like 2-3 nm particles were characterized. This result points to the relevance of surface effects. I would like to see a more elaborated discussion of these structural issues, e.g. on page 17. It is clear that this has to remain speculative but I am not convinced that the temperature profile aspects alone can explain the experimental findings in this and other studies.

---

**[Author reply]**

To the comment: I am still puzzled as to why the one experiments shows melting and the other one does not.:

Let me first explain how both the observation of ice vaporization without melting and that of ice melting can coexist without contradiction. Table 1 gives the summary of our observation: laser-induced events of ice microparticles (MPs) dependent on laser intensity.

**Table 1**. Laser-induced transformations observed for single ice MPs with diameters approximately 20 ~ 60 μm at temperatures between −10 and −15°C, together with calculated MP temperatures ($T_p$) during the illumination (outside temperature is set at −20°C in the calculation). This table was prepared based on both experimental results and calculated $T_p$. See ESI for the experimental results at low (ESI 6) and high (ESI 7) laser intensities and a list of calculated $T_p$ (ESI 8).

| laser power | phenomena | remark on $T_p$ (ESI 8 |
|---|---|---|
| ≥ 100 mW | fast and complete vaporization (ESI 7 | $T_p >> m_p$(ice) |
| 30~50 mW | Vaporization, supercooled droplet formation (Figs 5, 6, 7 | $T_p > m_p$(ice) |
| 10~20 mW | slow vaporization, no ice melting (ESI 6 | $T_p < m_p$(ice) |

Our main observation was supercooled water formation (Figure 5, 6, 7), along with vaporization that caused appreciable size reduction. However, as shown in Table 1, by reducing the laser intensity, we could observe only slow vaporization with no melting (please see ESI 6). At the same time, by increasing the laser intensity, we observed very fast and complete vaporization with no time for melting (please see ESI 7). Therefore, both vaporization without melting and melting accompanied by vaporization can be explained by the laser intensity effect for ice particles of

similar diameter. If the particle volume is bigger by a factor of $10^6$ (10 μm diameter vs. 1 mm diameter), particle heating can be extremely inefficient as can be expected from Fig 1 (b). This may explain why Richardson and coworkers failed to detect a liquid Raman peak because in their study water contained in a 3-mm ϕ × 3-mm-long well was frozen by cooling at −20°C. Also, their laser intensity might be weak because they used a moderately focused laser with an objective with a numerical aperture: 0.25-0.3 whereas we used a tightly focused laser with an objective of a numerical aperture, 0.7. This could give rise to 600 higher intensity ($W \cdot m^{-2}$) in our experiment than that of theirs for the same laser power (W).

Since we observed both melting and vaporization without melting within the framework of droplets supported on the same hydrophobic surface, dimethyldichlorosilane-treated glass surface (as described in the experimental section), depending on laser intensity, the surface effect may not be of primary importance. However, as suggested by the reviewer, we are willing to try other surfaces such as superhydrophobic surface in our future research.

We will add Table 1 as the summary of our observations with a new paragraph on page 24 in the new manuscript.

As mentioned above, Richardson's group used water contained in a 3-mm ϕ × 3-mm-long well that was frozen by cooling at −20°C, not a millimeter-sized particle on a substarte. Although we called their sample bulk ice, we could drop the expression "bulk" because it is not a critical issue.

---

**[Comments to the Author]**

2) The authors assign a slight change in the Raman spectrum (e.g. Fig. 5e) to a partially molten particle. How can you exclude that this shift is caused by an internal temperature change of the particle in the first time bin? The IR spectrum of water droplets shifts to the blue when the temperature increases. Please comment.

---

**[Author reply]**

In Figure 5e we observed, not spectral shift (as stated by the referee), but spectral shape change. In our Raman spectral observations, a peak at 3160 $cm^{-1}$ (ice peak) has practically no shifts as long as the ice phase exists at temperatures from the freezing point to at least −30°C. We could see no shift for the ice peak at 3160 $cm^{-1}$ in Figure 5a and Figure 7a,. We only observed increased intensities at regions 3300 – 3600 $cm^{-1}$, ascribable to liquid phase under laser illumination.

==========

Referee: 2

**[Comments to the Author]**

This paper describes the in-situ measurement of ice melting behavior by combining Raman

microscopy with focused near-IR beam irradiation as a point-heat source. The micrometer-sized ice particles under the laser irradiation showed the transition from solid to liquids, possibly, via supercooled water, which could not be detected by the past work about heating of ice crystals with photothermal effects of embedded plasmonic metal particles. They explained that the success of monitoring of the solid-liquid transition could be due to heat confinement in micrometer-sized ice particles. The experiments results are clear and potentially interesting to enhance the future technological development of the in-situ monitoring of ice melting behavior. However, I feel the interpretation about the obtained results is not well-summarized and thus this work sounds very inconclusive. These points should be improved in the revision for the further consideration of the publication in this journal.

---

**[Author reply]**

I really thank the referee for taking a painstaking task of reading our MS very carefully. Also thanks the referee for understanding that our result is useful for readers. Since the referee feel our interpretation is not enough, we will try our best to alleviate his/her concerns.

---

**[Comments to the Author]**

1: The reason why the focused near-IR laser beam was used in this study is not clear. They mentioned a lot about the past work of Richardson et al. using photothermal heating with plasmonic metal particles for ice melting in many parts of this paper including introduction. However, their description about the impact of this work was mainly focused on effects of ice particle size on heat confinement, which is not directly related to the reason of the change of heating methods to the focused near-IR laser beam. Although they mentioned a bit about the difficulty in making Au/NP/ice MP at the end of the discussion part of this paper, its reason was not explained, either. Since the use of the focused near-IR laser irradiation seems to be one of the crucial originalities of this work, the author should also clarify the characteristics (e.g., advantages and disadvantages) of the current heating method. For instance, are there any appropriate power, wavelength, and focus size to achieve the heat confinement?

---

**[Author reply]**

To the comment: The reason why the focused near-IR laser beam was used in this study is not clear: Because of weak light absorption by water molecules (absorption coefficient $\alpha$=0.14 $cm^{-1}$ at 1064 nm), we could observe melting of ice microparticles only by illuminating a focused 1064 nm laser light using a high numerical aperture microscope objective. This is because tightly focusing a Gaussian laser beam increases the laser power density (W $cm^{-2}$) by a factor of $10^6$ when using an objective with a numerical aperture of 0.7 (without the focused illumination, heating by laser was inefficient). Further, evaluation of the absorbed laser energy by water in the laser focal volume enabled the estimation of temperature increase by simulation (this point has been described in the Electronic Supporting Information, ESI 4)

To make this point clear, we added a paragraph that explains the merit of our laser illumination method in the beginning of subsection: *Laser-induced melting of single ice microparticles*, in the section of Results and Discussion.

To the comment: the author should also clarify the characteristics: appropriate power, wavelength, and focus size to achieve the heat confinement:

To meet the request by the referee, we added Table 1 (on page 24 in the new manuscript: subsection: *Sketch of melting by laser illumination*) that summarizes the laser intensity effect on the laser-induced transformation of ice microparticles to the revised manuscript. Because Table 1 includes the experimental observations at low and high laser powers besides an appropriate power given Figs. 5-7, such experimental data were given in ESI 6 and 7. A list of calculated $T_p$ is also given in ESI 8.

**Table 1**. Laser-induced transformations observed for single ice MPs with diameters approximately 20 ~ 60 μm at temperatures between −10 and −15°C, together with calculated MP temperatures ($T_p$) during the illumination (outside temperature is set at −20°C in the calculation). This table was prepared based on both experimental results and calculated $T_p$. See ESI for the experimental results at low (ESI 6) and high (ESI 7) laser intensities and a list of calculated $T_p$ (ESI 8).

| laser power | phenomena | remark on $T_p$ (ESI 8 |
|---|---|---|
| ≥ 100 mW | fast and complete vaporization (ESI 7 | $T_p >> m_p$(ice) |
| 30~50 mW | Vaporization, supercooled droplet formation (Figs 5, 6, 7 | $T_p > m_p$(ice) |
| 10~20 mW | slow vaporization, no ice melting (ESI 6 | $T_p < m_p$(ice) |

Our main observation was supercooled water formation (Figure 5, 6, 7), along with vaporization that caused appreciable size reduction. However, as shown in Table 1, by reducing the laser intensity, we could observe only slow vaporization with no melting. At the same time, by increasing the laser intensity, we observed very fast and complete vaporization with no time for melting. Thus, by presenting Table 1, we could show appropriate range for the observation of melting requested by the referee.

As has been described in ESI 4, Excitation laser wavelength is decisive for the absorption coefficient of ice because $Q = I\alpha$ (Q: heat generated at the laser spot, I: laser intensity, α: absorption coefficient of ice (water) at the laser wavelength) is the basic relationship of photothermal

conversion. Laser excitation wavelength is not decisive for our observation of the laser-induced melting (if the absorption coefficient is greater, we can observe the ice melting at lower laser intensity).

Laser focus size can be tuned nanoscale by using metal nanoparticles that strongly absorb laser light. This can be our future challenge as described in the text.

---

**[Comments to the Author]**

2: The COMSOL calculation in Figure 1 was carried out at the liquid water-air system (solid ice was not incorporated). Since Au particles were embedded in solid ice in the Richardson's works, I wonder whether the modeling of a water droplet that is surrounded by solid ice (and partially air?) should be appropriate.

---

**[Author reply]**

As suggested by the reviewer, Figure 1 (b) was replaced by a new one in which the initial condition of water is ice at −20°C (253 K). The melting enthalpy of fusion was included in the calculation. The result obtained is not much different although the absolute values of the temperature during laser illumination are slightly lower.

---

**[Comments to the Author]**

3: Figure 2 and Figure3:

Why was the critical temperature of ice nucleation for scattered droplets lower than that for densely-packed droplets. Can it be also explained by the Ostwald ripening?

---

**[Author reply]**

In our closed chamber, ice nucleation and growth of densely-packed droplets occurs in equilibrium with air that is supersaturated with respect to ice. Heterogeneous nucleation processes such as deposition nucleation (water vapor deposition), freezing nucleation (ice formation in supercooled droplet induced by outer ice nucleus) and ice-bridging (ice bridge growth from a frozen droplet to neighboring liquid droplets) have been characterized previously[*,**]. We observed similar phenomena. On the contrary, for scattered droplets, air inside the chamber may not be supersaturated because continuous shrinkage was observed for droplets. This can be a reason for the survival of supercooled water at −30°C.

[*]G. Vali1, P. J. DeMott, O. Möhler, and T. F. Whale, *Atmos. Chem. Phys*., 2015, **15**, 10263–10270.
[**]J. B. Boreyko and C. P. Collier, *ACS Nano* 2013, **7**, 1618–1627.

We added this statement in the new manuscript.

On page 7:

"In our closed chamber, ice nucleation and growth of densely-packed droplets occurs in equilibrium with air that is supersaturated with respect to ice. Heterogeneous nucleation processes such as deposition nucleation (water vapor deposition), freezing nucleation (ice formation in supercooled droplet induced by outer ice nucleus) and ice-bridging (ice bridge growth from a frozen droplet to neighboring liquid droplets) have been characterized previously. As described above, we observed phenomena similar to the previous investigations."

On page 9:

scattered droplets are difficult to handle because they suffer gradual size reduction and finally disappear, possibly because of evaporation "into the chamber atmosphere that may not be supersaturated."

---

**[Comments to the Author]**

4: Figure 5(a) and (e):

According to Figure 5 (a), there seems to be a drastic change of the spectral shape between t = 100 (light blue) and 110 (orange), which may be attributed to the change from supercooled water to water according to the Raman spectra. However, as far as my understanding is correct, the peak analysis of the Raman data at t = 110 and 120 was not shown in Figure (e) where the Bin starting time ended at 100-110. If so, it would be interesting to add the bins of t = 110 and 120 in Figure 5(e), which may show much higher the ratio (I3360/I3160) and thus clarify the detection of the three different regimes (solid ice, supercooled water, and water) by the in-situ Raman spectroscopy.

---

**[Author reply]**

The referee's point, "adding the bins of t = 110 and 120 in Figure 5(e)", is quite intriguing. However, because we could not see Raman peaks at 3160 $cm^{-1}$ for the bins of t = 110 and 120, the ratio (I3360/I3160) can be too big to be included in Figure 5(e). This the reason why we excluded the Raman data at t = 110 and 120 from Figure 5(e).

---

**[Comments to the Author]**

5: From line 17, p. 17

The author mentioned about some points that were not incorporated in the COMSOL calculation of Figure 8. Could the author assess the impact of each point (major or minor) on the interpretation about the results of this paper? In addition, should one also take into account about the density of water droplets on substrate (densely-packed or scattered)?

---

**[Author reply]**

To the comment: Could the author assess the impact of each point (major or minor):

The most important issue is whether the calculated temperature distribution using the heat transfer equation is reliable. This cannot be answered unless we actually measure the temperatures of ice

particles during the laser illumination. Our future research is heading for this direction. At this moment, we just made clear the approximations we used for temperature estimation using COMSOL.

We add a description, “Although our calculated temperatures well explain the present observation of ice melting, temperature measurements are needed for ice particles during the laser illumination to show the validity of temperatures obtained by simulation.”, on page 21.

To the comment: should one also take into account about the density of water droplets on substrate:

In our experiment, only a single ice particle was subjected to focused laser illumination. As a result, no melting/vaporization was observed for ice particles around the particle of interest. For precaution, each measurement was performed for an isolated ice particle by illuminating a focused (~1 μmϕ) laser. Thus, “densely-packed or scattered” does not matter here. In the scattered case, it was difficult to find ice particles even at −30°C because many droplets stayed as supercooled liquid as has already been described (see Fig. 3 and description related on page 9).

We added this description to the blue lines on page 13.

---

# Melting of a single ice microparticle on exposure to focused near-IR laser beam to yield a supercooled water droplet†

Shuichi Hashimoto *[a] and Takayuki Uwada[b]

[a] Advanced Engineering Course, NIT Gunma College, 580 Toriba-machi, Maebashi, Guma 371-8530, Japan. E-mail: hashichem@gunma-ct.ac.jp orcid.org/0000-0002-8020-5537

[b] Department of Chemistry, Josai University, 1-1 Keyakidai, Sakado, Saitama 350-0295, Japan. E-mail: uwada@josai.ac.jp orcid.org/0000-0003-4272-7964

†Electronic supplementary information (ESI) available. See DOI: https://doi.org/10.1039/

Abstract

We observed for the first time that a single ice microparticle supported on a substrate melted photothermally to form a supercooled water droplet on exposure to tightly focused illumination with a 1064-nm laser beam that generated a point heat source. In-situ Raman micro-spectroscopy clearly showed the formation of liquid water at the expense of ice. The observation of this melting is only possible when the experiment is performed with micrometer-sized ice particles. A previous attempt to melt millimeter-sized ice through photothermal heating of gold nanoaggregates fell short of expectations because only vapor formation, rather than liquid water formation, has been postulated. Our observation is significant because thermal confinement in a microscale compartment using a water-air interface as a heat-insulated wall can achieve particle temperatures above the melting point of water, whereas, in an unlimited space of ice, heat transfer from the heating center to the surroundings causes steep temperature decays, resulting in limited temperature increase.

## Introduction

Photothermal heating phenomena through light-to-heat conversion at nano- and microscales have attracted considerable attention because there are many potential applications[1], including photothermal cancer therapy and drug delivery[2,3]. The concept central to photothermal responses is temporal and spatial propagation of heat generated at a pinpoint location, referred to as heat transfer or heat dissipation[4,5]. The heat transferred to the surroundings is the origin of various intriguing phenomena associated with photothermal effects, including temperature shaping[6], temperature confinement[7], and optothermofluidic motions[8] (e.g. convections and thermo-diffusions).

Photothermal heating-induced small-scale phase transitions have been pursued for the medium adjacent to plasmonic nanoparticles. Notably, the liquid-to-gas phase transition, or boiling of water within several nanometers away from gold nanoparticles (Au NPs), has been elucidated thanks to the feasible detection of nano- and microbubbles through optical scattering imaging and spectroscopy. Both time-dependent and steady-state observations have been made[9-15] and the elaborate dynamics of bubbles have been investigated: from early generation (fs~ps) to final collapse (ns~μs)[10,11]; unusual bathtub-shape Au NP size-dependent laser energy thresholds[11,13]; and the onset of bubble generation at spinodal temperature (~500 K) in superheated water, but not at normal boiling temperature (373 K)[15]. In contrast, less attention has been paid to the photothermally-induced melting of ice, the solid-to-liquid phase transition of water. In attempting to investigate photothermal ice melting, a major obstacle is the lack of a suitable method to detect the phase change sensitively particularly at small volumes. Additionally, to study the melting transition of water, temperature control is required for optical microscopy, although photothermal bubbles have been studied at ambient temperature.

Nevertheless, as early as 2006, Richardson and coworkers published a seminal paper describing their attempt to melt ice through photothermal heating of gold nanoaggregates (Au NAs)[16,17]. However they provided insufficient evidence of liquid water formation as a result of using laser beam illumination on millimeter-sized ice contained in a 3-mm ϕ × 3-mm-long well. On

continuous irradiation with a 532-nm laser, a Raman signal indicative of ice was merely weakened but was not replaced by a new signal indicating the presence of liquid water. They ascribed their observation to the heating-induced sublimation of the ice.

A question arises as to why the sublimation of ice occurs without first melting to the liquid state. Their experimental result is here interpreted differently by proposing that bulk ice acts as a heat sink of infinite volume that immediately quenches heat at interfaces with Au NAs and transfers it to the surrounding area. The greater thermal conductivity of ice (2.2 W $m^{-1}$ $K^{-1}$) than that of liquid water (0.6 W $m^{-1}$ $K^{-1}$) may facilitate this process. This heat transfer may suppress the melting of ice in the close vicinity of the heating spot. However, if an ice particle of finite volume is used instead of bulk ice, heat transfer may be affected. To investigate this hypothesis, a modeling calculation was performed using the FEM software package COMSOL Multiphysics (www.comsol.jp). **Figure 1**a shows a geometrical model of the COMSOL calculation. The model consists of a spherical ice particle (d=2, 10, 16 μm), surrounded by air, within which a 100-nm diameter Au NP was embedded at the center. For comparison, the calculation was also performed with the bulk ice of volume 125,000 $\mu m^3$ (50 μm×50 μm×50 μm).

When the central Au NP is optically heated, radial heat transfer immediately follows from the Au NP to water and then to the air. The resulting steady-state radial temperature distribution is shown in Figure 1b, from which a number of deductions can be made. Firstly, COMSOL predicts that temperature confinement can be achieved in a droplet levitated in air because of a sudden drop in thermal conductivity at the interface between water (0.6 $Wm^{-1}K^{-1}$) and air (0.02 W $m^{-1}$ $K^{-1}$). Contrastingly, in bulk ice, temperature decayed out at small distances within less than a micrometer from the center. Secondly, smaller-diameter droplets maintain a higher temperature. This suggests that, if the photothermal heating experiment is performed for a Au NP contained a micro-sized ice at temperatures below the freezing temperature, there is a good chance of observing photothermal ice melting under this condition in contrast to bulk ice.

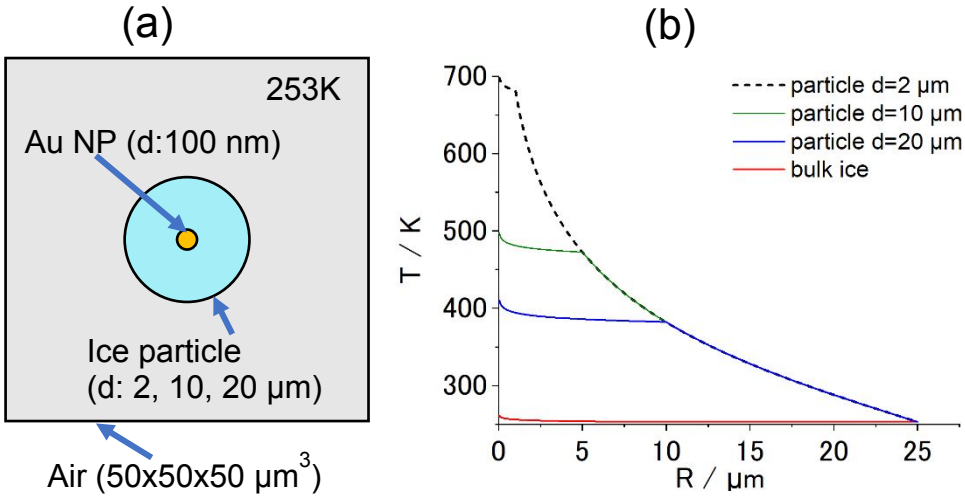


**Figure 1** (a) COMSOL calculation geometry. The calculation cell consisted of a cubic air space of volume 50 μm×50 μm×50 μm at the center of which were placed spherical ice particles of various radii, including a 100-nm diameter Au NP at the center. The temperature of the cell was set to 253 K (−20°C). A focused illumination (FWHM of the laser spot: 1.0 μm) with a 532-nm laser beam was performed with a power of 1.0 mW. The latent heat of fusion for ice at 0°C was considered in the calculation. (b) Curves of calculated temperature, T, vs. distance from the center, R. Temperature discontinuities were observed at the boundary of the water droplet with air.

Based on the predictions obtained from the above COMSOL calculation, a microparticle-based photothermal experiment was performed. To mimic the NP-light interaction to generate a point heat source, focused illumination with a NIR laser was employed to generate a microscale heating spot.

**Experimental Section**

The single-particle Raman spectra were measured using the experimental configuration illustrated in **Scheme 1**. Wavelength resolution was 0.5 nm on a spectrophotometer consisting of a SP-2300*i* polychromator (Acton Research, MA) with a grating of 300 grooves/mm blazed at 500 nm and a CCD camera (DU401-BR-DD; Andor Technology, Belfast, UK; operated at −60°C), measured through a pinhole (view area: 10-μm diameter). Wavelength calibration of the spectrograph was performed using Ne lines as a reference. A focused 532-nm DPSS laser (GL523T3; Laser Century, Shanghai, China) was used for excitation (3.5 mW) when recording the Raman spectra. The particles were heated by illumination with the focused beam of a 1064-nm CW laser (MIL-H-1064-3W; CNI, Changchun, China) through a microscope objective (60×, NA = 0.70) on an inverted microscope (IX-71; Olympus, Tokyo, Japan). The two laser beams were introduced collinearly using a dual-band dichroic mirror (Edmund Optics Japan, Tokyo). *In-situ* Raman spectra were collected for 100 − 200 s using 10-20 multiple exposures of 10 s each. The time-dependent spectral evolution was represented by overlaying the spectral signal at every 10 s.

Water droplets were generated from distilled water or 0.1 M aqueous $CaCl_2$ solution using a nebulizer (NESCOSONIC UN-511; Alfresa Farma, Osaka, Japan) and deposited on a 0.17-mm-thick borosilicate cover glass (Matsunami Glass, Osaka, Japan). Hydrophobized glass surfaces were prepared by immersion in a solution of 5% dimethyldichlorosilane (TCI, Tokyo, Japan) in toluene for 30 min and washing copiously with methanol. The lateral view of a hemispherical droplet on the hydrophobized glass surface is shown in the inset of Scheme 1. The droplet-covered surfaces of two cover glasses were opposed using a 0.2-mm-thick silicone spacer, thus containing the droplets within a closed chamber.

Custom-installed dual $N_2$-gas flow lines were used to cool the sample chamber and to minimize fogging. A dry nitrogen stream, cooled by being first passed through a liquid nitrogen container, was introduced into a cooling chamber covered with a polystyrene foam thermal insulator. The sample chamber was attached to the bottom of the cooling chamber. The $N_2$-gas flow for

defogging was applied to the space between the sample bottom and the objective. For temperature monitoring, two T-type thermocouples were taped to the sample chamber, one on each side. The cooling rate was 0.3 − 0.4 °C $min^{-1}$.

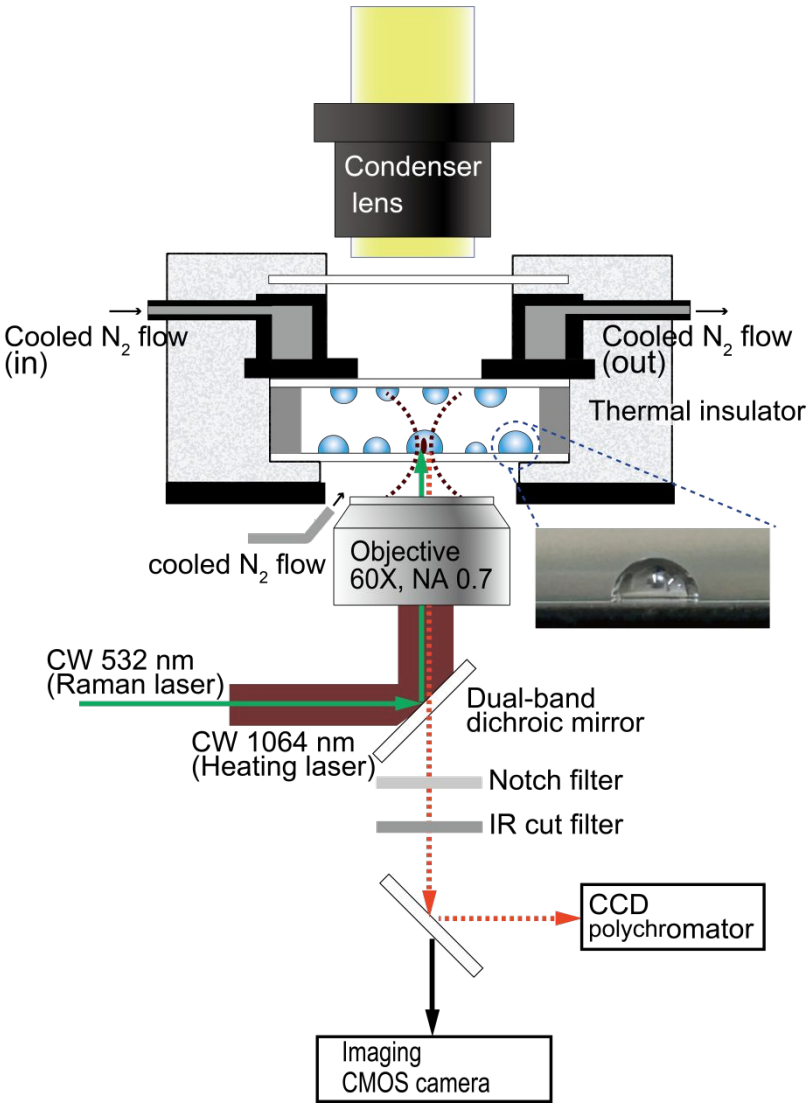


**Scheme 1** Experimental configuration.

## Results and Discussion

*Ice-microparticle formation from water droplets*

Ice microparticles (MPs) were prepared from water droplets supported on a cover glass in a closed chamber, as depicted in Scheme 1. **Figure 2** shows sequential images of cooling for droplets prepared densely on the substrate. In Fig. 2a, all droplets in the field of view are liquid. Comparison of Figs. 2a and b (identical imaging area) reveals that many ice particles had just formed in Fig. 2b at −5°C. The ice particles can be identified by small bumps and dips on the surface. For such densely prepared droplets as in Fig. 2, the onset of freezing occurred abruptly at temperatures ranging approximately between −2 and −7°C depending on the sample. Fig. 2c shows that, with time, ice MPs undergo size growth as well as forming interconnected structures. This observation suggests that in ice formation, moisture evaporated from droplets in the chamber plays a crucial role. As shown in Fig. 2d, further growth occurred with time and some particles grew significantly larger in volume than that of original droplets at the expense of other particles. That is, the Ostwald ripening phenomena occurred[18]. Such dynamic growth events are exemplified in **ESI 1**. In our closed chamber, ice nucleation and growth of densely-packed droplets occurs in equilibrium with air that is supersaturated with respect to ice. Heterogeneous nucleation processes such as deposition nucleation (water vapor deposition), freezing nucleation (ice formation in supercooled droplet induced by outer ice nucleus) and ice-bridging (ice bridge growth from a frozen droplet to neighboring liquid droplets) have been characterized previously[19-20]. As described above, we observed phenomena similar to the previous investigations.

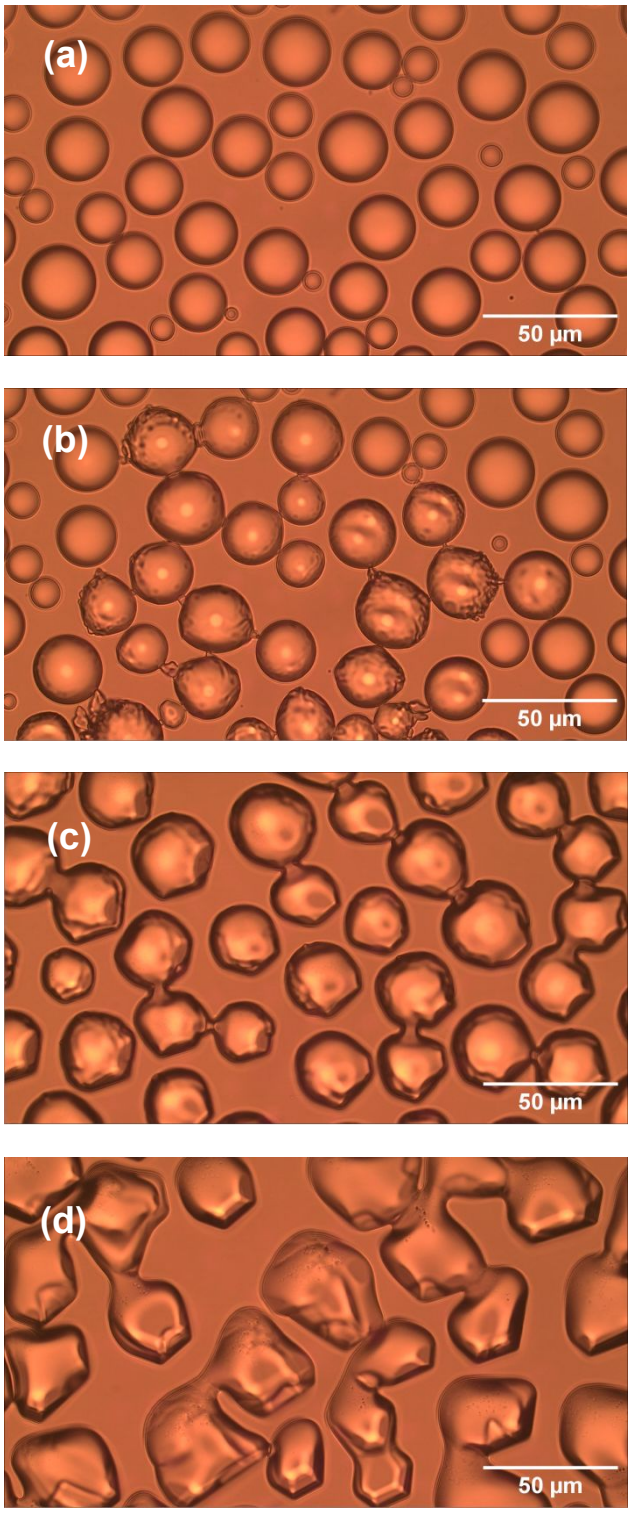


**Figure 2**. Sequential images of droplet cooling. (a) Liquid water droplets at −5°C. (b) Onset of crystallization at −5°C in the same area as in (a). (c) Growth and interconnection of ice microparticles occurred as time progressed (−8°C after 6 min). (d) Further growth of ice particles with time (−10°C after 20 min).

It has been shown previously that supercooled water MPs on solid surfaces crystallize at temperatures close to the homogeneous nucleation temperature of −38°C, which is considered to be the ultimate limit of supercooling[19-26]. For instance, Li and coworkers have shown, by observing the opacity of each droplet, that the onset of ice nucleation occurred at −39°C for droplets of 14.5 − 66.7 μm supported on silicon wafers[19]. Using video microscopy, Murray and coworkers observed the onset of ice formation at −36°C for 10 – 40 μm droplets deposited on hydrophobic $(CH_3)_2Cl_2Si$-coated glass[20]. Although approximately 10°C higher, Mael and coworkers obtained the onset of nucleation at −26.5 ± 0.9°C, as observed by Raman microscopy, for water droplets on hydrophobically-coated quartz discs[21]. As shown in **Fig. 3**, when the density of droplets was decreased, the supercooled droplets survived at temperatures as low as −25°C. **Figure 3** shows particle image and Raman spectra for scattered droplets at temperatures of −5, −10, and −25°C. The Raman spectra of these droplet had the characteristics of the liquid phase (details below)[27-29], surviving in this state down to at least −30°C. This result is analogous to observations by others[23]. However, scattered droplets are difficult to handle because they suffer gradual size reduction and finally disappear, possibly because of evaporation into the chamber atmosphere that may not be supersaturated. Thus, ice particles were prepared from densely-packed droplets.

It was possible to observe the progress of freezing from liquid water, by Raman spectroscopy at −10°C, as shown in **Fig. 4**a. Figure 4b shows the particle image of a liquid droplet before the measurement, and Fig. 4c shows the same particle after crystallization. The Raman spectra of water in the OH-stretching region provide insight into the phase information. Ice spectra exhibit a pronounced peak at 3140 – 3160 $cm^{-1}$ with a less-pronounced contribution from the 3200 to 3600 $cm^{-1}$ region; whereas liquid water shows a broad band with a maximum at 3400 $cm^{-1}$ and a shoulder at 3200-3250 $cm^{-1}$ at ambient temperatures[23,27,30,31]. The contribution of the shoulder intensity is temperature-dependent and increased with lowering of the temperature. For supercooled water, the contribution of the region at 3200 $cm^{-1}$ markedly increased relative to the peak at 3400 $cm^{-1}$, compared with that at ambient temperature (see **ESI 2**), and formed another peak (Fig. 3

right). This observation was consistent with previous findings for liquid water[22-26]. In Fig. 4a, the ice peak at 3160 $cm^{-1}$ suddenly appeared at 70-80 s while the liquid spectrum was observed at 50-60 s, suggesting that freezing of a liquid droplet was completed in 10 to 20 s. The next step is to experiment with laser illumination.

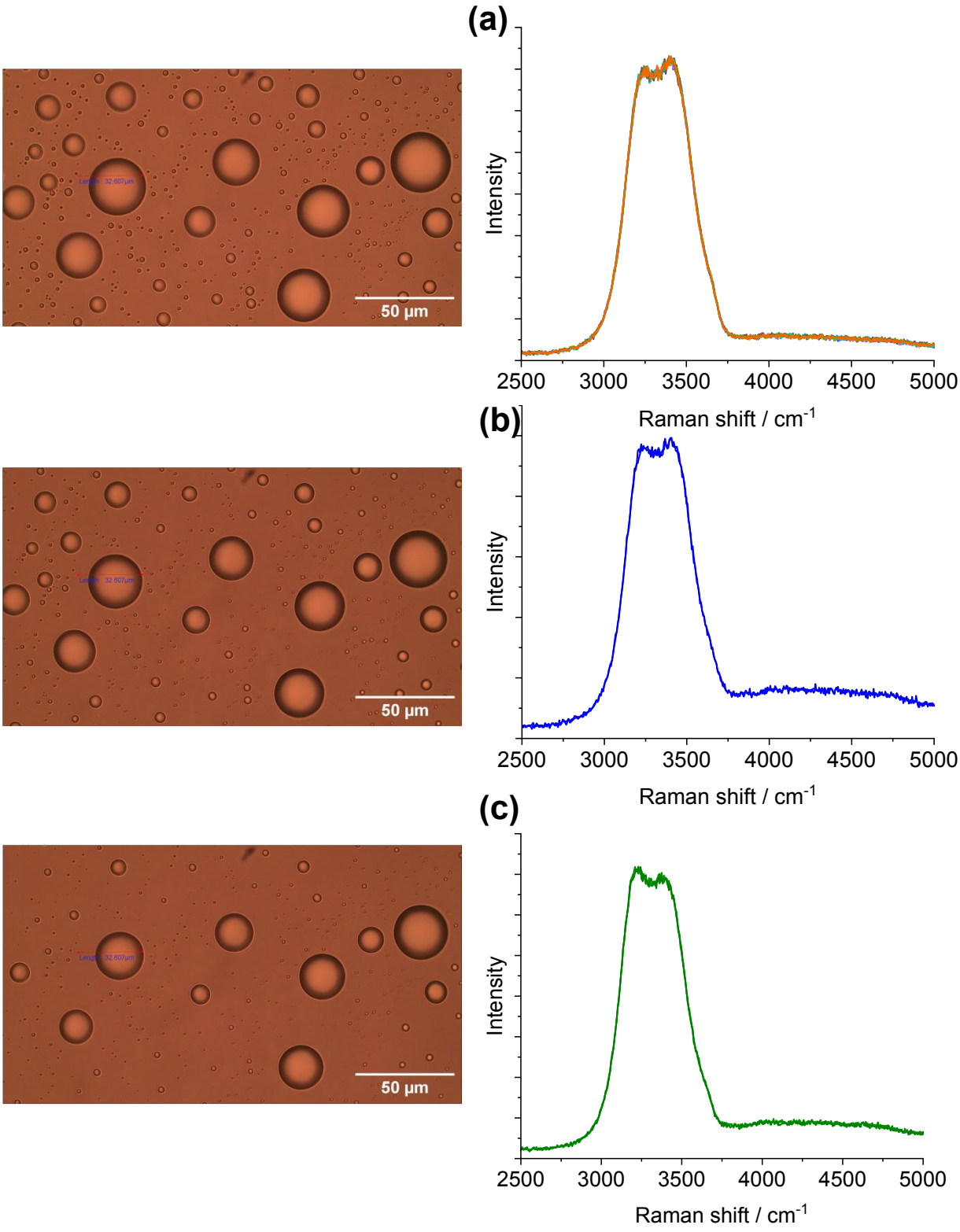


**Figure 3**. Images (left) and Raman spectra (right) of supercooled microdroplets scattered on substrates at three different temperatures: (a) −5°C, (b) −10°C, (c) −25°C. Raman spectra were ascribed to those of liquid water, showing that droplets failed to crystallize even at −25°C.

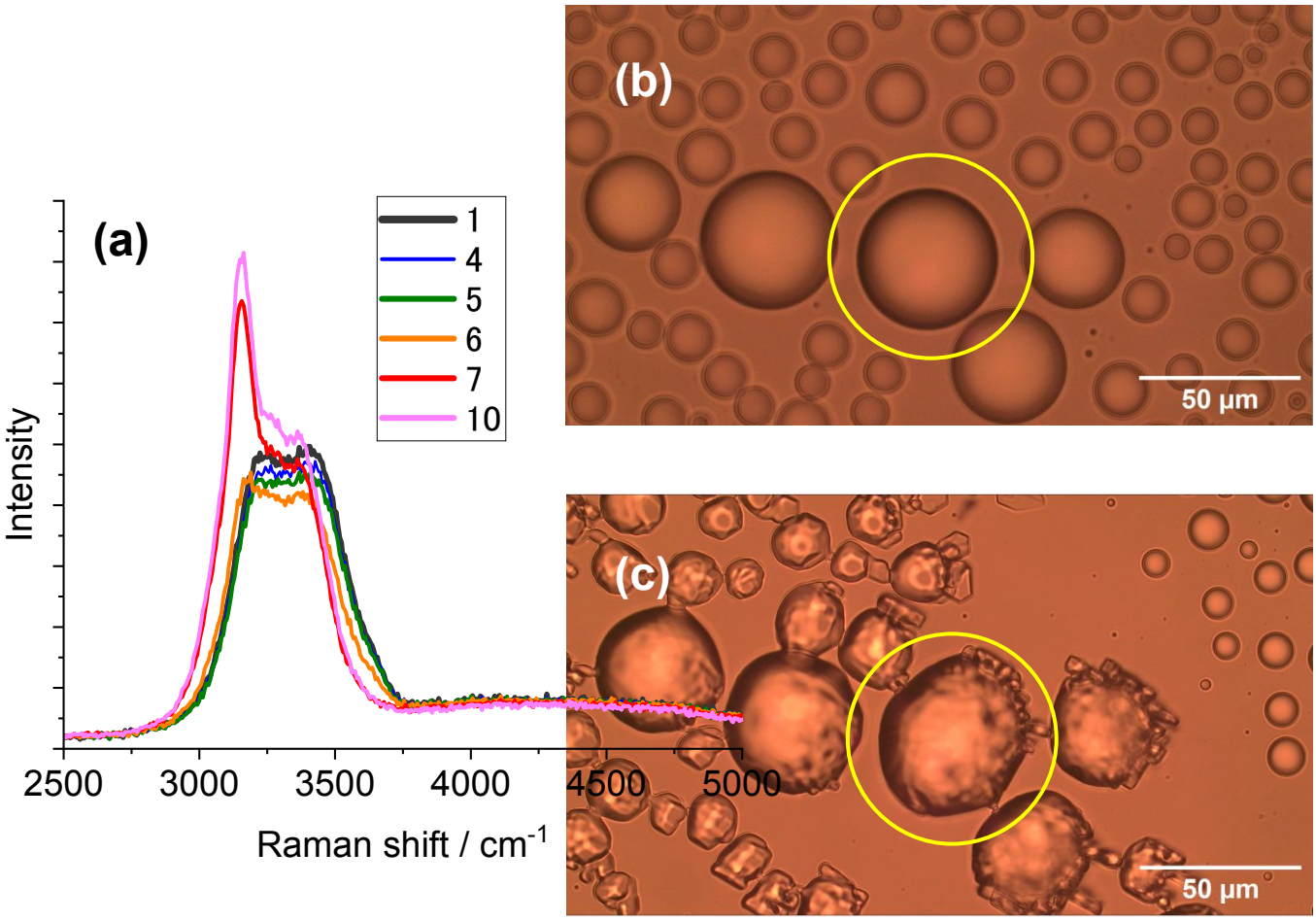


**Figure 4** (a) Real-time observation for single particle Raman spectral evolution of a droplet freezing at −10°C. (b, c) Images of a supercooled droplet before the Raman spectroscopic measurement (b) and image of ice particles (c) after the measurement. Raman spectral measurements were performed for the particle encircled. The spectral numbers represent the bin numbers of the spectral accumulation (1, 0-10 s; 4, 30-40 s; 5, 40-50 s; 6, 50-60 s; 7, 60-70 s; 10, 90-100 s).

*Laser-induced melting of single ice microparticles*

~~Using focused illumination with a 1064-nm laser, the intention was to generate a high-temperature spot in a single ice MP thereby driving heat transfer throughout the particle and to the surrounding air, which may eventually lead to ice melting. As observed from the Raman spectral evolution of ice crystallization in Fig. 4, it was anticipated that it should be possible to detect the reverse process, ice to liquid water, induced by the laser~~. Because of a weak light absorption by water molecules at 1064 nm (absorption coefficient $\alpha$=14.2 $m^{-1}$ [32]), we could observe melting of ice MPs only by illuminating a focused light using an objective of numerical aperture: 0.7. This is because, for the same laser power (W), tightly focusing a Gaussian laser beam increases the laser power density (W $cm^{-2}$) by a factor of 600 when using an objective with a numerical aperture of 0.7 compared with using that with a numerical aperture of 0.3. Further, evaluation of the absorbed laser energy by water molecules in the laser focal volume enabled the estimation of temperature increase by calculation. In our experiment, only a single ice particle was subjected to focused laser illumination. As a result, no melting/vaporization was observed for ice particles around the particle of interest. For precaution, each measurement was performed for an isolated ice particle for focused (~1 μm ϕ) laser illumination.

**Figure 5** shows *in-situ* Raman spectra during laser illumination (Fig. 5a), along with particle images before and after exposure (Fig. 5b, c), and finally the Raman spectrum of the residual particle (Fig. 5d). Simultaneously, the intensity ratio of 3360 $cm^{-1}$ to 3160 $cm^{-1}$, $I_{3360}/ I_{3160}$, from each spectrum in Fig. 5a was plotted in Fig. 5e as a function of bin starting time, BST. This ratio serves as a good measure for ice melting because, if and when melting occurs, the liquid peak is expected to increase at the expense of the ice peak. Inspection of Figure 5a reveals that initially the contribution of the ice peak (3140-3170 $cm^{-1}$) is dominant but later is replaced by the signal of liquid water (BST 110, 120). Comparison of the images in Fig. 5b and 5c indicates that particle volume was markedly reduced, and transformed into a sphere of diameter ~ 1 μm. As the Raman spectrum 5 min after illumination (Fig. 5d) is that of liquid, it is reasonable to assume that a

supercooled liquid droplet is formed. The Raman spectrum of the liquid water stayed unchanged over a prolonged period. This result is consistent with the survival of supercooled droplets at temperatures above −25 to −30°C (see Fig. 3).

Now follows a close inspection of the spectral shape changes with exposure time (Fig. 5e). Initial laser illumination produced a slight but distinct increase in the value of $I_{3360}/I_{3160}$ (see the difference between BST −10 and 0). As this increase resulted from laser-heating, the Raman change suggests that the ice particle underwent partial or incomplete melting. During illumination, the ratio stayed nearly constant until 80-90 s, after which a distinct increase was observed. Then, the ice peak disappeared and the Raman spectrum originated entirely from liquid (BST 110,120). During illumination, the particle size was markedly reduced presumably because of vaporization that may deprive the particle of thermal energy. Thus, regardless of initial ice particle size, the laser heating primarily causes vaporization of ice together with partial melting and finally complete melting occurs.

The vaporization rate depended on the chamber temperature as well as the laser intensity and exposure time. For instance, when the temperature was −6°C, a liquid droplet formed and disappeared quickly because of a high vaporization rate. By contrast, when the temperature was below −20°C, a size-reduced ice particle was left because of a low rate of vaporization. At temperatures between −10 and −15°C, the liquid droplet formed did not disappear in most cases. The vaporization rate is much more pronounced for partially melted droplets formed from ice particles subjected to laser illumination. Such an observation is shown in **Fig. 6**. From the Raman spectra in Fig. 6e, it is assumed that the particle in Fig. 6b has partially melted (BST 0.68) and that the particle in Fig. 6d is a liquid droplet. An appreciable size reduction was observed after 6 min at −14°C (from Fig. 6b to Fig. 6d) because of vaporization. Images in Figs. 6b-d captured the transition from partial to complete melting.

To minimize the vaporization of droplets, the vapor pressure of water was reduced by adding salt. Figure 7a shows clearly the gradual spectral alteration from the ice spectrum before

illumination (EST −10), then to ice-dominant spectra (BST 0,10,20), and finally to liquid spectra (BST 70, 80, 90). In 0.1M $CaCl_2$, the melting of ice particles proceeded as the exposure time increased (Fig. 7d), because of a much reduced vaporization rate. The resultant liquid droplet diameter was ~ 10 μm (Fig. 7c), much greater than that found after illumination of pure water (Fig. 5c). By adding a salt, the heating-time dependent increase in the extent of melting was clearly observed.

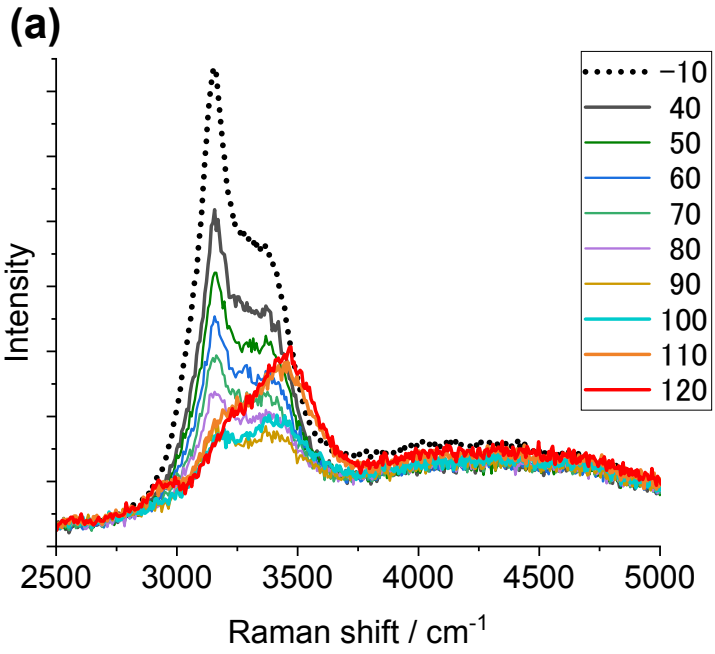
(a)
Intensity
−10
40
50
60
70
80
90
100
110
120
2500
3000
3500
4000
4500
5000
Raman shift / cm-1

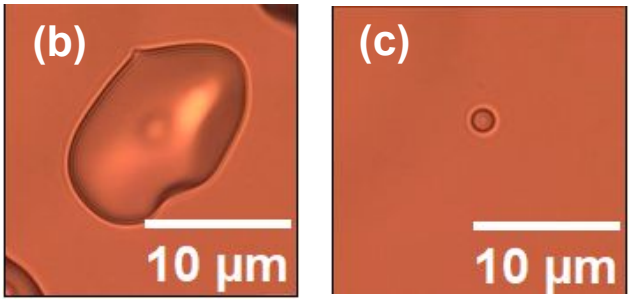
(b)
10 μm
(c)
10 μm

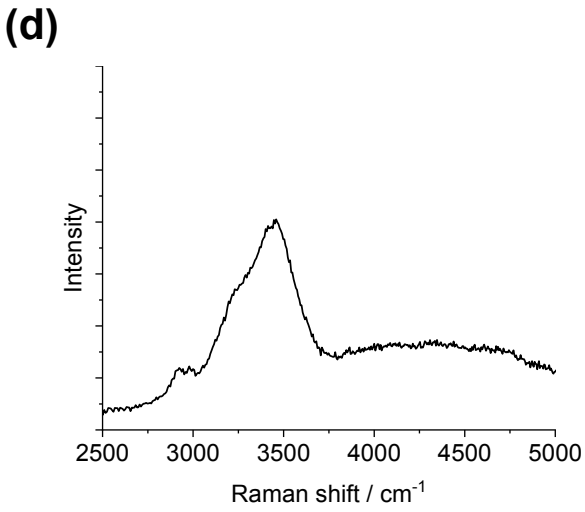
(d)
Intensity
2500
3000
3500
4000
4500
5000
Raman shift / cm-1

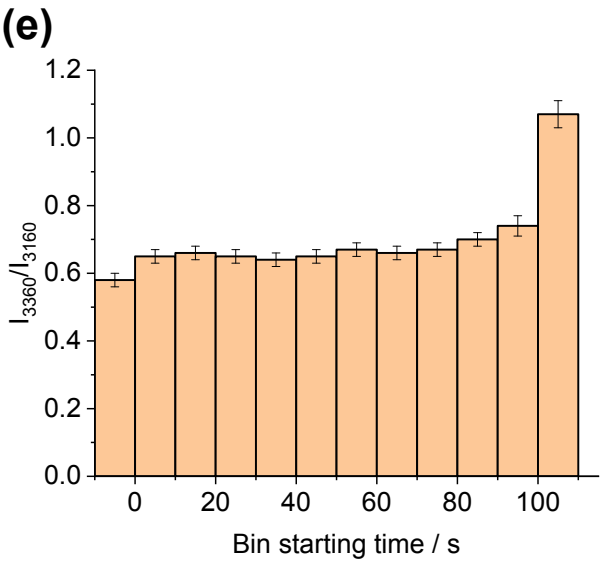


**Figure 5** (a) Raman spectral evolution on exposure to laser illumination (1064 nm, 30mW) of a single ice particle at −15°C. Raman spectra were acquired every 10s. (b, c) Particle images before (b) and after (c) illumination. (d) Raman spectrum of the droplet in (c) when left for 5 min after illumination. (e) Spectral shape changes represented by $I_{3360}/I_{3160}$ vs. starting bin time. In a, the number for each spectrum is the bin starting time (BST). Also, a spectrum corresponding to a number −10 (dotted line) represents the spectrum before laser illumination, the intensity of which was adjusted to fit into the figure. In a, broad background signals between 3000 and 5000 $cm^{-1}$ are ascribed to luminescence from the glass substrate.

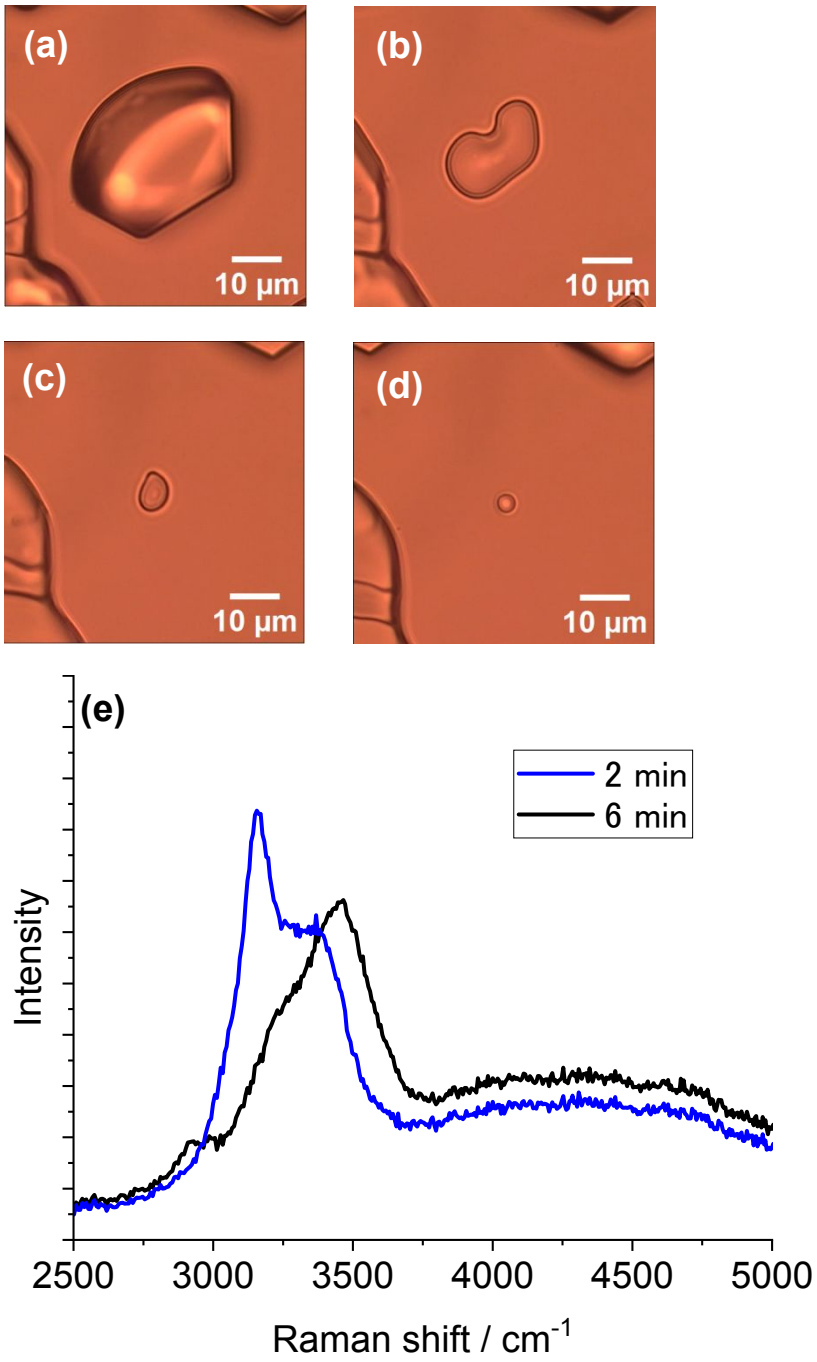


**Figure 6**. Observation of vaporization from a laser-induced melting particle and related Raman spectra. (a) Ice particle before laser illumination. (b) Partially melted ice particle after 60 s of laser illumination of the ice particle in (a). (c) Particle image 2 min after image (b). (d) Droplet image 6 min after (b). (e) Raman spectra acquired from the particle in (b) (blue line, BST 0.68) and (d) (black line). *In-situ* Raman spectra (1064 nm, 50 mW) after image in a and before image in b was given in Supporting Information ESI 3. The environmental temperature was −14°C.

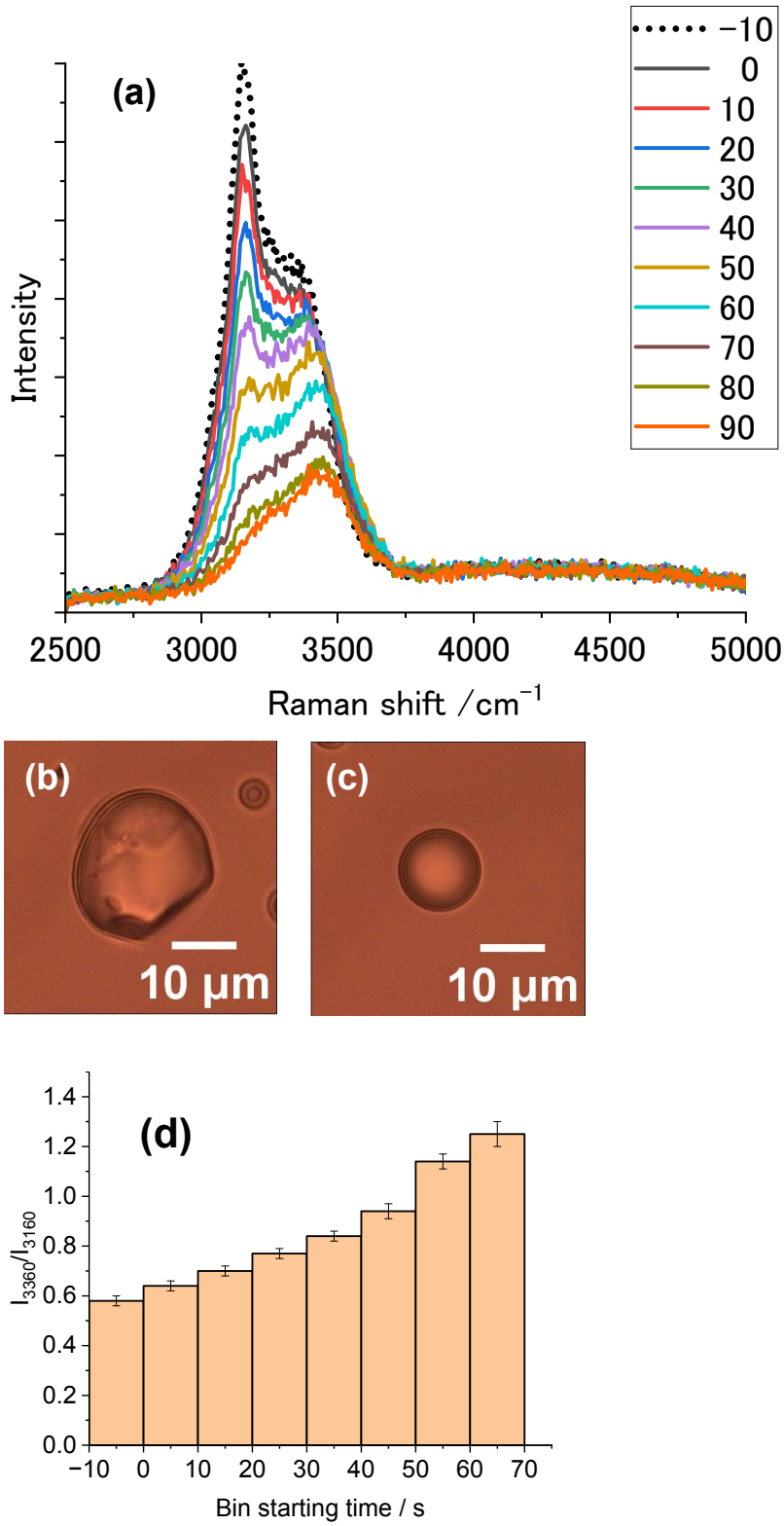


**Figure 7**. (a) Raman spectral changes every 10 s for a single ice particle containing 0.1 M $CaCl_2$ during 1064-nm laser illumination (50 mW) at −12°C. The spectrum corresponding to −10 (dotted line) is that before laser illumination commenced. (b, c) Particle images before (b) and after (c) illumination. (d) $I_{3360}/I_{3160}$ vs. BST for the spectra in (a).

*COMSOL calculations*

Laser light at 1064-nm is absorbed by OH-vibrational overtones, which results in heat generation in water at the focus[33]. The absorption coefficient ($\alpha$) of liquid water has been reported as 14.2 $m^{-1}$ [32] and the same value applies to ice[34]. Using the heat transfer equation[5,35], we calculated temperature distribution at various points inside the sample chamber resulting from the focused laser illumination followed by heat transfer (**Fig. 8)**. Considering the latent heat of fusion for ice at 0°C, temperatures were calculated based on illumination with laser light at 50 mW output (details of the COMSOL calculation are provided in **ESI 4**).

The COMSOL calculation suggests that heat transfer occurs from the particle center at the laser focus to the outer areas in the chamber (Fig. 8a, b). One-dimensional temperature decay is clearly shown in Fig. 8c and an expanded view inside the particle (Fig. 8d) shows that the decay has a discontinuity at the water/air boundary. This boundary suppresses heat dissipation, enabling a temperature increase of the ice particle above the freezing point. From the temperature confinement point of view, using a substrate for supporting the particles is disadvantageous, because this substrate cannot prevent heat dissipation from ice to the glass surface. Most importantly, if bulk ice is used instead of MPs, such temperature confinement cannot be achieved (**ESI 5**).

There are some additional points that were not incorporated in the calculation. In COMSOL, a whole spherical particle shape was used as a model. In reality, ice particles of various shapes were generated from the original hemispherical droplets. Heat transfer to the substrate is more efficient with a hemispherical particle (**ESI 5**), but the calculation suggests that this hemisphere can result in raising the temperature above the freezing point. Although exact conditions at the contact area between ice particles and the substrate are uncertain, ice-substrate contact will influence the effectiveness of heat transfer to the substrate. Also, calculations did not take account of the observed gradual shrinking of the particles due to vaporization during illumination. Additionally, a laser spot spheroid of size 1 μm × 5 μm was estimated from consideration of a spatial resolution at the laser focus (**ESI 4**). However, because the laser light intensity changes continuously, there is

uncertainty in determining the exact focal spot size. Despite these defects, the validity of the basic concept of temperature confinement in an ice particle is expected to result in a reasonable approximation by the COMSOL calculation based on the heat transfer model. Although our calculated temperatures well explain the present observation of ice melting, temperature measurements are needed for ice particles during laser illumination to show the validity of temperatures obtained by simulation.

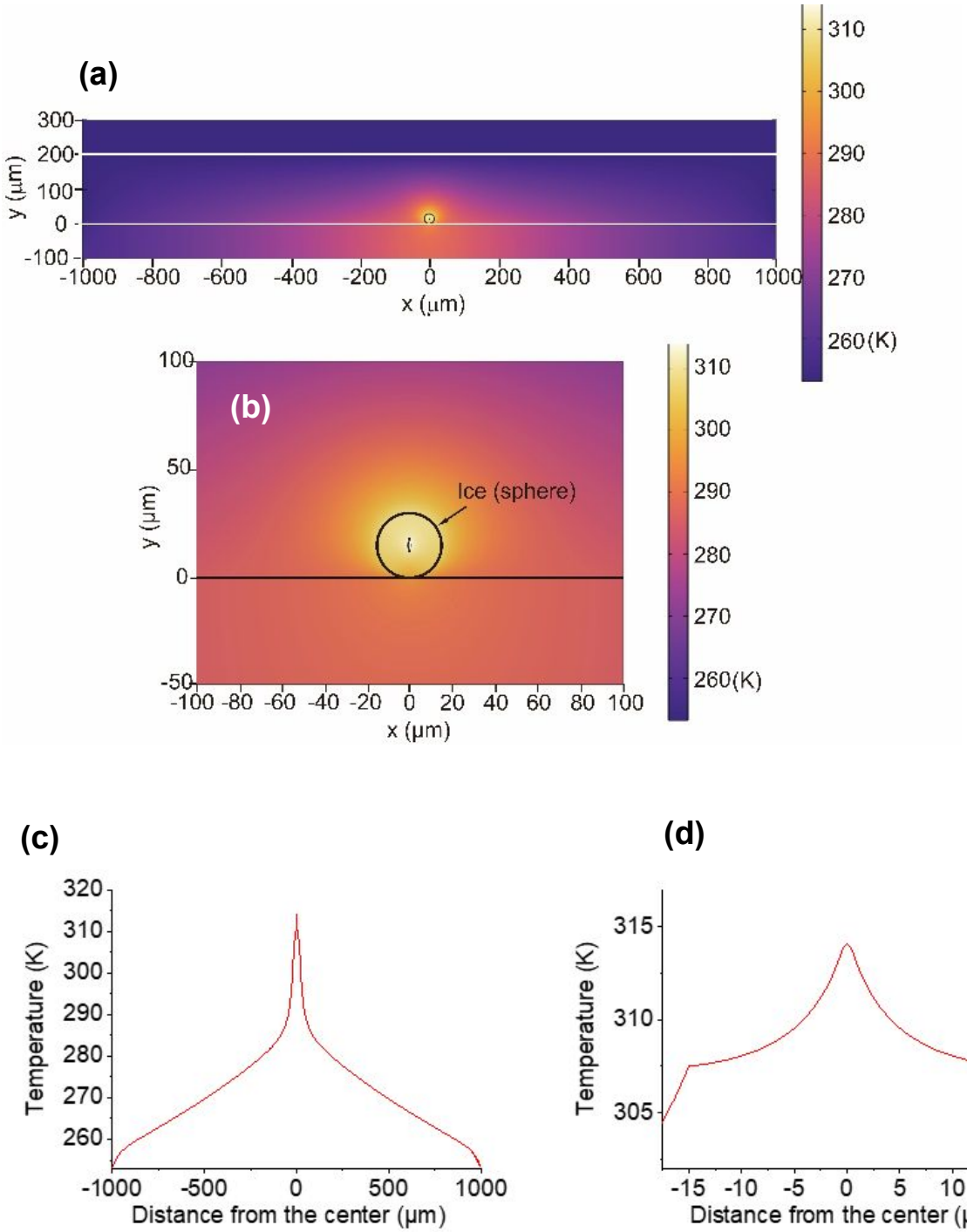


**Figure 8** Temperature distribution in a sample chamber (formed by the space between two glass substrates separated by a 200 μm spacer) during illumination with a 1064-nm laser (50 mW). (a) Ice particle of diam. = 30 μm supported on a substrate. (b) Expanded image of (a). (c) 1D temperature distribution on the equator in the horizontal direction. (d) Horizontal expansion from the graph in (c). The chamber wall temperature was fixed at −20°C (253 K).

*Sketch of melting by laser illumination*

The laser-heating-induced melting of single ice MPs was observed but the underlying mechanism is not straightforward. Notably, when heated, ice particles of 20−30 μm tend to undergo surface vaporization that strongly retards particle melting (Fig. 5). This vaporization leads to size reduction which enables more efficient heating. When the size is < 10 μm, complete melting was observed by Raman spectroscopy, which is supported by the round-shaped particle images. Adding $CaCl_2$ to droplets was found to result in marked suppression of ice vaporization (compare Figs. 5 and 7), the effect of which enabled observation of the transformation of the ice to supercooled liquid. ~~The present experiments furnished evidence of ice vaporization as seen by particle size reduction in the images, while Richardson and coworkers merely assumed the sublimation of bulk ice incorporating Au NAs when illuminated with a 532-nm laser[13,14], ascribing their observation of the decrease in the Raman ice peak intensity to sublimation (**ESI 6**). The approach in the present study revealed that bulk ice is disadvantageous because of the lack of heat confinement, which may explain why Richardson and coworkers failed to detect a liquid peak.~~ Here we summarize the present observation of laser-induced ice transformations depending on both laser power and particle diameter in Table 1.

**Table 1**. Laser-induced transformations observed for single ice MPs with diameters approximately 20 ~ 60 μm at temperatures between −10 and −15°C, together with calculated MP temperatures ($T_p$) during the illumination (outside temperature is set at −20°C in the calculation). Table 1 was prepared based on both experimental results and calculated $T_p$ (experimental results at low (ESI 6) and high (ESI 7) laser intensities and for a list of calculated $T_p$ (ESI 8)).

| laser power | phenomena | remark on $T_p$ (ESI 8 |
|---|---|---|
| ≥ 100 mW | fast and complete vaporization (ESI 7 | $T_p >> m_p$(ice) |
| 30~50 mW | Vaporization, supercooled droplet formation (Figs 5, 6, 7 | $T_p > m_p$(ice) |
| 10~20 mW | slow vaporization, no ice melting (ESI 6 | $T_p < m_p$(ice) |

Our main observation was supercooled water formation (Figs 5, 6, 7), along with vaporization that caused appreciable size reduction. Moreover, by reducing the laser intensity, we could only observe slow vaporization with no melting (ESI 6). At the same time, by increasing the laser intensity, we observed very fast and complete vaporization with no time for melting (ESI 7). Therefore, both vaporization without melting and melting accompanied by vaporization can be explained by the laser intensity effect for ice particles of similar diameter (ESI 8). If the particle volume is much bigger, for instance, by a factor of $10^6$ (10 μm diameter vs. 1 mm diameter), particle heating can be extremely inefficient as can be expected from Fig 1 (b). This may explain why Richardson and coworkers failed to detect a liquid Raman peak[16,17] because, in their study, water contained in a 3-mm ϕ × 3-mm-long well was frozen by cooling at −20°C (ESI 9). Note that their laser intensity might be weak because they used a moderately focused laser beam with an objective with a numerical aperture: 0.25-0.3.

Thermodynamically, the supercooled liquid-to-ice transition is described by a metastable to stable state conversion with an activation barrier[36]. From classical nucleation theory, ice clusters nucleate in liquid water and crystallization results when the clusters grow to a critical size to overcome the activation barrier at constant temperature and pressure[32]. In contrast, ice melts by

illumination under non-equilibrium conditions and a steady-state temperature gradient will be formed, as simulated by COMSOL in Fig. 8. The temperatures inside the particle were estimated to be above the equilibrium freezing temperature. Melting proceeded only when particles became small and were hampered by vaporization. The morphology of partially or incompletely melted particles is assumed to involve a liquid-core/ice-shell structure according to the temperature profile simulated with COMSOL (Fig. 8d). Hence, a free-energy curve for stable ice to metastable liquid may not be the reverse of crystallization. Further discussion is beyond the scope of this study.

In the present study, real-time Raman observation of crystallization from liquid water (Fig. 4) was achieved at a constant temperature. A Raman excitation laser (3.5 mW, $\alpha$=0.0447 $m^{-1}$ at 532 nm[38]) was introduced only for observation, not as a stimulus for crystallization. Strikingly, Yoshikawa and coworkers have observed that ice crystallization in supercooled water can be stimulated by a femtosecond laser[39]. An effective multiphoton excitation at the laser focus generates shockwaves and bubbles, which can act as an impulse for inducing ice crystal nucleation. Femtosecond laser impulses allowed the transition from a metastable to a stable crystalline state by overcoming the activation barrier. Importantly, the present study provided observation of the ice-to-liquid transition induced by thermal heating through CW laser illumination, which is in contrast to the observation of liquid-to-ice transition using femtosecond laser irradiation[39]. This ice-to-liquid transition is possible because supercooled water can exist at temperatures above −38ºC.

The preliminary goal of the present study was to achieve the melting of ice MPs by heating with a focused laser illumination. However, the primary objective is to melt ice MPs incorporating a Au NP (Au NP/ice MP) using the photothermal effect of Au NP, which may enable much higher temperatures. To this end, ice MPs incorporating a Au NP are required. At the present time we have not yet succeeded in preparing AuNP/ice MP. Furthermore, using levitated ice MPs is challenging but preferred in photothermal heating experiments because this would provide the idealized thermal isolation illustrated in Fig. 1a.

## Conclusion

In the past decade, photothermal heating using plasmonic nanoparticles/nanostructures or, simply, thermoplasmonics has been successful in confining and shaping a heating spot at nanoscale. However, at larger scales, heat transfer must be regulated because otherwise temperature decays cannot be controlled, and heat generated can be wasted without being used efficiently. In this study, it was demonstrated that introducing a heat-insulating interface is markedly effective in interfering with temperature decays and thus managing the heat transfer. Photothermal-heating-induced melting of ice microparticles was observed to result in supercooled water droplets at temperatures below the equilibrium freezing temperature of water. Note, however, that a previous study on the melting of ~~bulk~~ millimeter-sized ice using plasmonic photothermal heating did not work as expected because of heat dissipation. The method of heat confinement in terms of compartmentalization reported here needs further refinement. Using a substrate to support ice microparticles can be an obstacle to suppressing heat transfer. A better method might be to levitate ice particles using optical trapping. Further research is under way.

## Author Contributions

S.H. performed optical measurements and analyzed the data. T. U. performed the simulation. S.H. conceived and designed the experiment. S.H. wrote the manuscript with a contribution from T. U. All authors have approved the final version of the manuscript.

## Conflicts of Interest

The authors declare no competing financial interests.

## Acknowledgments

Financial support from JSPS KAKENHI (Grant No.22K04884, and No.23K04541) is gratefully acknowledged.

**References**


1. G. Baffou, F Cichos, and R. Quidant, *Nature Mat*. 2020, **19**, 946–958.
2. M. R. K. Ali, Y. Wu, and M. A. El-Sayed, *J. Phys. Chem.* C 2019, **123**, 15375−15393.
3. M. Sharifi, F. Attar, A. A. Saboury, K. Akhtari, N. Hooshmand, A. Hasan, M. A. El-Sayed, and M. Falahati, *J. Controlled Release* 2019, **311−312**, 170−198.
4. S. Hashimoto, D. Werner, and T. Uwada, *J. Photochem. Photobiol. C: Rev*. 2012, **13**, 28–54.
5. A. O. Govorov and H. H. Richardson, *Nano Today* 2007, **2**, 30–38.
6. C. Molinaro, M. Bénéfice, A. Gorlas, V. Da Cunha, H. M. L. Robert, R. Catchpole, L. Gallais, P. Forterre, and G. Baffou, *Nature Commun*. 2022, **13**, 5342.
7. W. Sheng, S. He, W. Seare, and A. Almutairi, *J. Biomed. Optics*, 2017, **22**, 080901.
8. Z. Chen, J. Li, and Y. Zheng, *Chem. Rev*. 2022, **122**, 3122−3179.
9. C. Boutopoulos, A. Hatef, M. Fortin-Deschênesa and Michel Meunier, Nanoscale, 2015, 7, 11758–11765.
10. A. Siems, S. A. L. Weber, and A. Plech, *New J. Phys*. 2011, **13**, 043018.
11. T. Katayama, K. Setoura, D. Werner, H. Miyasaka, and S. Hashimoto, *Langmuir* 2014, **30**, 9504−9513.
12. L. Hou, M. Yorulmaz, N. R. Verhart, and M. Orrit *New J. Phys.*2015, **17** 013050.
13. K. Metwally, S. Mensah, and G. Baffou, *J. Phys. Chem.* C 2015, **119**, 28586−28596.
14. Y. Wang, M. E. Zaytsev, H. L. The, J. C. T. Eijkel, H. J. W. Zandvliet, X. Zhang, and D. Lohse, *ACS Nano* 2017, **11**, 2045–2051.
15. G. Baffou, J. Polleux, H. Ringeault, and S. Monneret, *J. Phys. Chem*. C 2014, **118**, 4890−4898.
16. H. H. Richardson, Z. N. Hickman, A. O. Govorov, A. C. Thomas, W. Zhang, and M. E. Kordesch, *Nano Lett*. 2006, **6**, 783–788.
17. H. H. Richardson, A. C. Thomas, M. T. Carlson, M. E Kordesch,. And A. O. Govorov, *J. Electron. Mater*. 2007, **36**, 1587–1593.

18. C. Solans, P. Izquierdo, J. Nolla, N. Azemar, and M. J. Garcia-Celma, *Current Opinion Colloid Interface Sci*. 2005, **10**, 102–110.

19. G. Vali1, P. J. DeMott, O. Möhler, and T. F. Whale, *Atmos. Chem. Phys*., 2015, **15**, 10263–10270.

20. J. B. Boreyko and C. P. Collier, *ACS Nano* 2013, **7**, 1618–1627.

21. K. Li, S. Xu, W. Shi, M. He, H. Li, S. Li, X. Zhou, J. Wang, and Y. Song, *Langmuir*, 2012, **28**, 10749–10754.

22. B. J. Murray, S. L. Broadley, T. W. Wilson, S. J. Bull, R. H. Wills, H. K. Christenson, and E. J. Murray, *Phys. Chem. Chem. Phys.* 2010, **12**, 10380–10387.

23. L. E. Mael, H. L. Busse, and V. H. Grassian, *Anal. Chem.* 2019, **91**, 11138−11145.

24. T. Inada, H. Tomita, and T. Koyama, *Interfacial J. Refrig*. 2014, **40**, 294−301.

25. J. Atkinson, B. Murray, and D. O'Sullivan, *J. Phys. Chem.* A 2016, **120**, 6513−6520.

26. K. K. Tanaka and Y. Kimura, *Phys. Chem. Chem. Phys*. 2019, **21**, 2410–2418.

27. L. E. Mael, G. Peiker, H. L. Busse, and V. H. Grassian, *J. Phys. Chem*. A 2021, **125**, 10742−10749.

28. S. Ishizaka, T. Wada, and N. Kitamura, *Chem. Phys. Lett.* 2011, **506**, 117−121.

29. C. Q. Sun, X. Zhang, X. Fu, W. Zheng, J-I. Kuo, Y. Zhou, Z. Shen, and J. Zhou, *J. Phys. Chem. Lett*. 2013, **4**, 3238−3244.

30. I. Duriˇckovi´c, R. Claverie, P. Bourson, M. Marchetti, J-M. Chassot, and M. D. Fontana, *J. Raman Spectrosc*. 2011, **42**, 1408−1412.

31. X. Xue, Z. Z. He, and J. Liu, *J. Raman Spectrosc*. 2013, **44**, 1045−1048.

32. J. G. Erwin, F. G. Peterman, and C. F. Schmidt, *Biophys. J*. 2003, **84**, 1308–1316.

33. S. Ishizaka, J. Ma, T. Fujiwara, K. Yamauchi, and N. Kitamura, *Anal. Sci*. 2016, **32**, 425−430.

34. S. G. Warren, *Phil. Trans. R. Soc.* A 2019, **377**, 20180161.

35. G. Baffou, R. Quidant, and F. J. Garcı´a de Abajo, *ACS Nano*, 2010, **4**, 709–716.

36. A. F. Henegham, P. W. Wilson, G. Wang, and A. D. J. Haymet, *J. Chem. Phys*. 2001, **115**, 7599−7609.

37. N. Maeda, *Molecules* 2021,**26**, 392.

38. R. M. Pope and E. S. Fry, *Appl. Opt*. 1997, **36**, 8710–8723.

39. H. Takahashi, T. Kono, K. Sawada, S. Kumano, Y. Tsuri, M. Maruyama, M. Yoshimura, D. Takahashi, Y. Kawamura, M. Uemura, S. Nakabayashi, Y. Mori, Y. Hosokawa, and H. Yoshikawa, *J. Phys. Chem. Lett*. 2023, **14**, 4394−4402.

Graphical Abstract (8 × 4 cm)

The use of micro-Raman spectroscopy revealed that the laser-heating-induced melting of ice microparticles results in supercooled liquid droplet formation where the liquid state occurred at temperatures below the freezing point of water. The result was interpreted by thermal confinement in a microscale compartment using a water-air interface as a heat-insulated wall, enabling particle temperatures above the melting point of water.

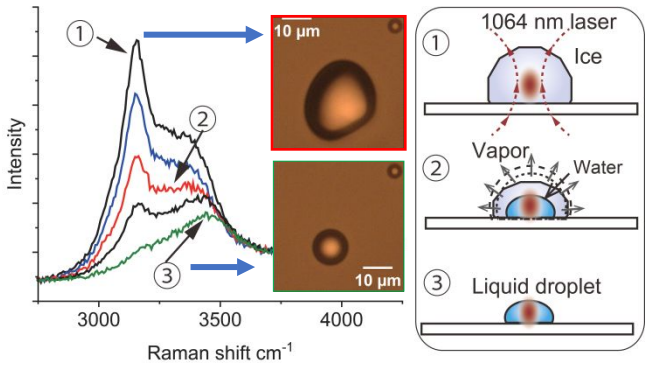

Electronic Supplementary Information

# Melting of a single ice microparticle on exposure to focused near-IR laser beam to yield a supercooled water droplet

Shuichi Hashimoto*[a] and Takayuki Uwada[b]

[a] Advanced Engineering Course, NIT Gunma College, 580 Toriba-machi, Maebashi, Gunma 371-8530, Japan,

[b]Department of Chemistry, Josai University, 1-1 Keyakidai, Sakado, Saitama 350-0295, Japan.

**ESI 1. Propagation of droplet crystallization**.

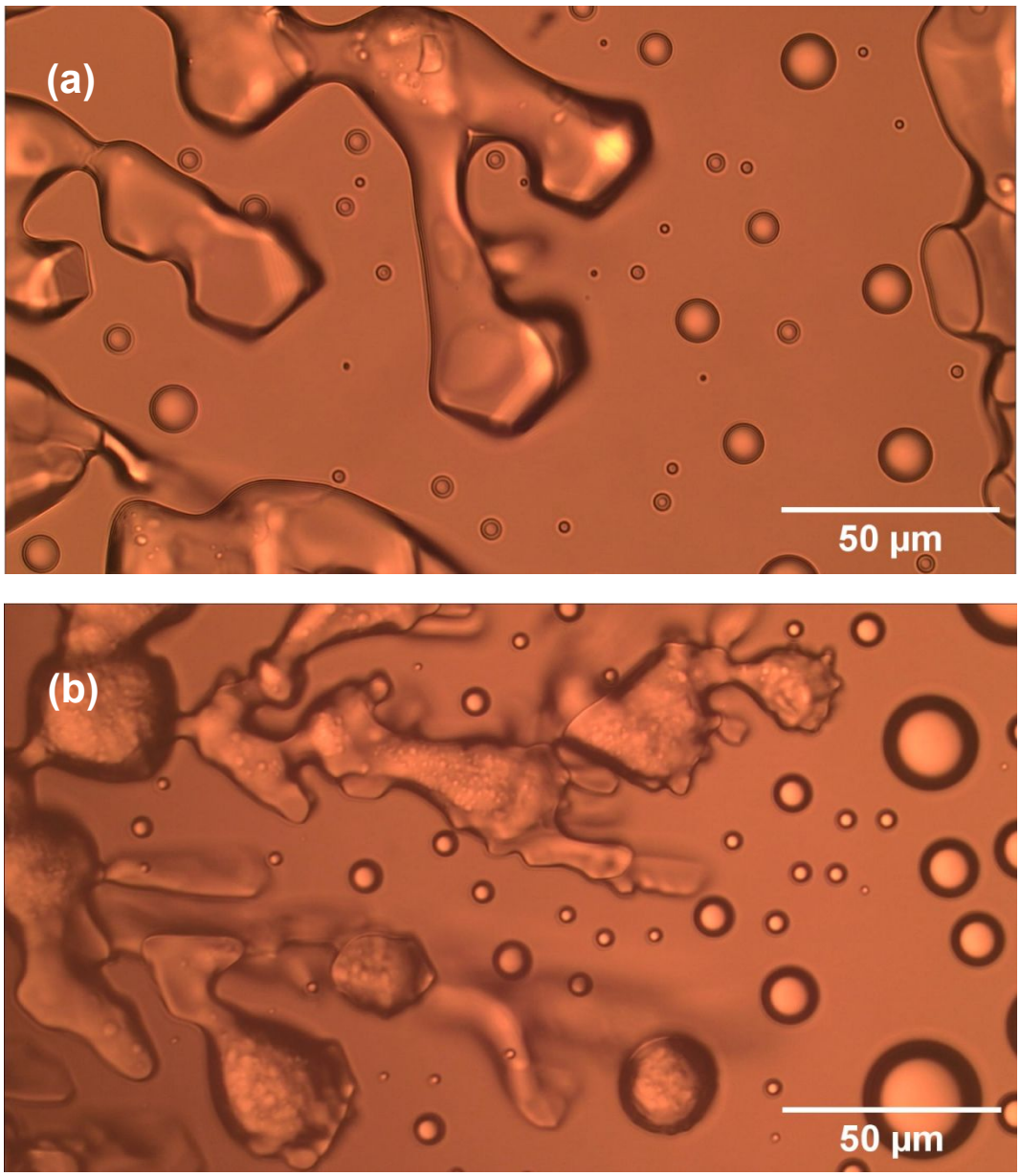


**Figure S1** (a), (b) During the ice crystallization, dynamic growth was observed by capturing droplets, forming connected and large structures.

**ESI 2. Raman spectra of a water droplet at various ambient temperatures.**

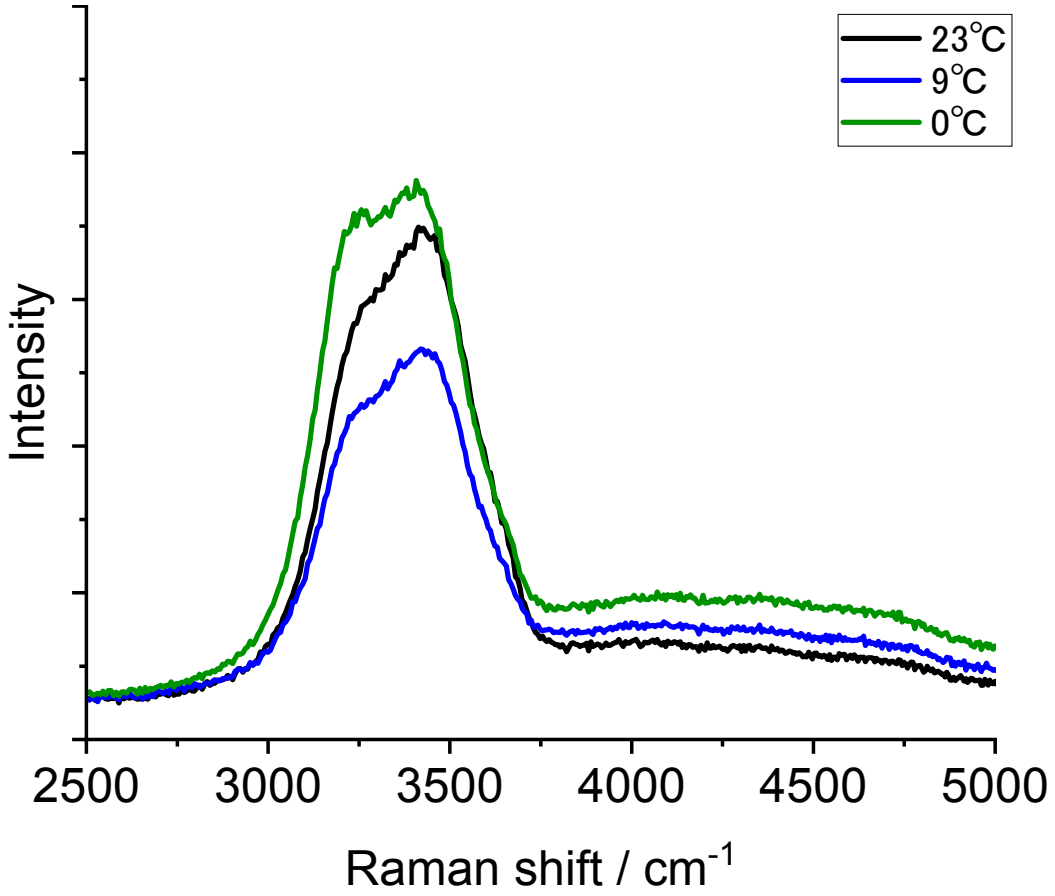


**Figure S2** Comparison of Raman spectral shapes were made at three temperatures: 23, 9, 0°C.

**ESI 3. In-situ Raman spectra for Figure 6.**

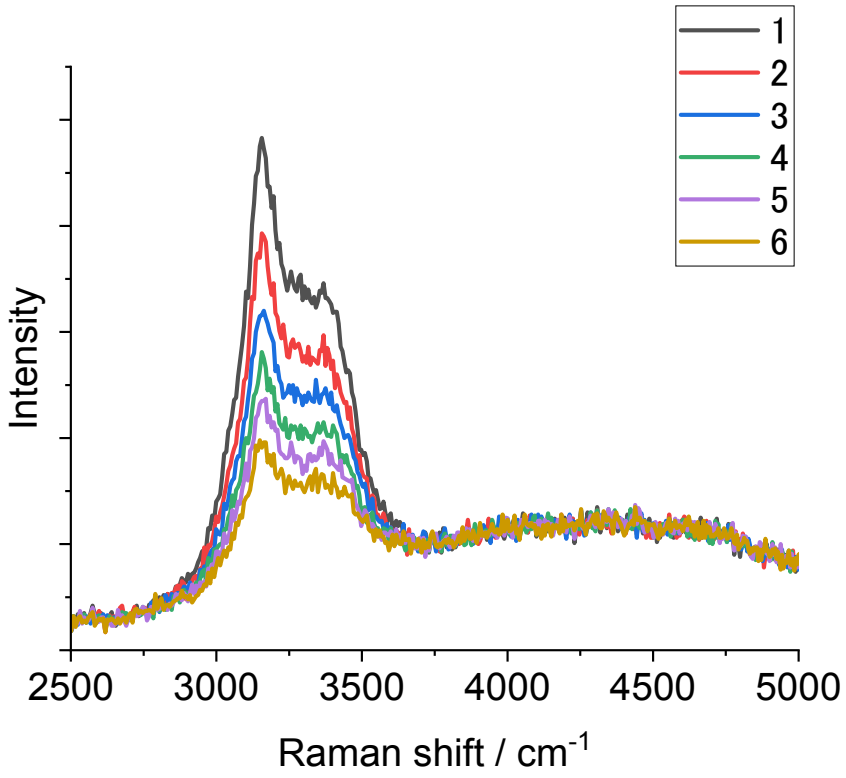


**Figure S3** Single particle Raman spectral evolution associated with Figure 6 on exposure to laser illumination (1064 nm, 50mW) of a single ice particle at −15°C. Raman spectra were acquired every 10s. The spectral numbers represent the bin numbers of the spectral accumulation (1, 0-10 s; 4, 30-40 s; 5, 40-50 s; 6, 50-60 s).

**ESI 4. Numerical simulation using COMSOL.**

A commercial finite-element mode solver, COMSOL Multiphysics Ver. 6.0 (http://www.comsol.com), was used for temperature estimation under illumination of a focused laser beam on an ice microparticle (MP). The schematic illustration of simulation geometry built for COMSOL is shown in Figure S3a. All the elements: the ice MP (30-μm diameter sphere or hemisphere), air layer, and glass substrates (upper and lower) were included in the model based on the experimental configuration. At the center of the ice MP, we placed an elliptical spot representing a laser spot. The lengths of the minor and major axes for the laser spot were determined by the full width at half maximum (FWHM) intensity of the laser spot on the basis of lateral and axial resolutions[1].

$$(\text{lateral resolution})\ \frac{0.51\lambda}{\text{NA}} \qquad (\text{axial resolution})\ \frac{2n\lambda}{\text{NA}^2}$$

where λ is the wavelength of a laser (1064 nm), n is the refractive index of the surrounding air (1.0), and NA is the numerical aperture of the objective lens (0.6). Physical properties of ice, air, and glass substrates such as thermal conductivity, viscosity, and heat capacity, and density were taken from the COMSOL Material library[2].

The heat generation by laser illumination was assumed to be triggered by the absorption of light at the laser spot, i.e., the elliptical spot in ice MP. The absorption coefficient of ice (water), α, at 1064 nm was taken from the literature[3], 0.14 $cm^{-1}$, and the heat generated at the laser spot, Q, was calculated with the following equation[4].

$$Q = I\alpha$$

where I represents the intensity of the laser beam, which is defined as the average of the incident laser power at the elliptical volume that acted as a heat source. Next, we calculated the temperature distribution in a chamber using the heat transfer module[5]. As an initial condition, the temperature distribution in the model was assumed to be uniform and equal to 253 K. The heat is continuously generated upon the laser illumination and is transferred to the surrounding, resulting in an increased

steady-state temperature distribution throughout the chamber. Time-dependent heat transfer in the model is expressed by the following equation[5]:

$$\rho C_P \left( \frac{\partial T(\mathbf{x},t)}{\partial t} + \mathbf{u}(\mathbf{x},t) \cdot \nabla T(\mathbf{x},t) \right) = \nabla \cdot \left( k \nabla T(\mathbf{x},t) \right) + Q(t)$$

where T(**x**, t) is temperature at arbitrary position **x** at time t, ρ is the mass density, $C_P$ the specific heat capacity at the constant pressure, **u**(**x**, t) the fluid velocity vector, k the thermal conductivity of the system at the position **x**, and Q(t) is the energy deposition term. In this case, the temperature elevation in the ice MP is supposed to exceed a phase transition temperature of ice at 273.15 K. Thus, we considered the latent heat of fusion and change of physical properties at the phase transition temperature. The detail of the phase change is described in the application note "Phase Change" released by COMSOL[6]. In the calculation, the value of latent heat of fusion, 333.5 kJ $kg^{-1}$ and that of the transition interval, 10 K were used. The temporal change of the temperature at the top of the ice is shown in Figure S3b. Because of the heat transfer from the laser spot, the temperature of ice is increased with time but we can find a small step around 270 K from 0 to 0.2 s, indicating the heat dissipation by the latent heat of fusion. The temperature reached a steady-state approximately at 3 s after the laser illumination. The maximum temperature was calculated as 314 K.

For hemispherical ice MP, which is akin to the observed droplet shape, we calculated the heat transfer from the laser spot and temperature elevation in the same manner. The temperature distribution map around the hemispherical ice upon laser illumination is shown in Figure S5a. The laser power was set to 50 mW. At the top of the ice, the temperature reached 297 K, which is lower than that of spherical ice. This temperature suppression occurred from heat dissipation to the glass substrate because of a greater contact area.

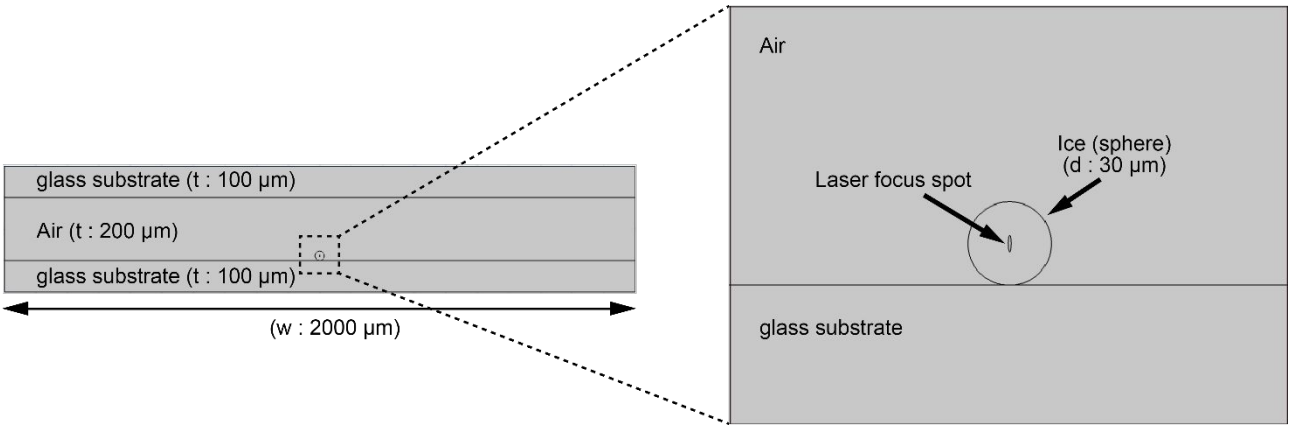


**Figure S4 (a)** Schematic illustration of the simulation geometry.

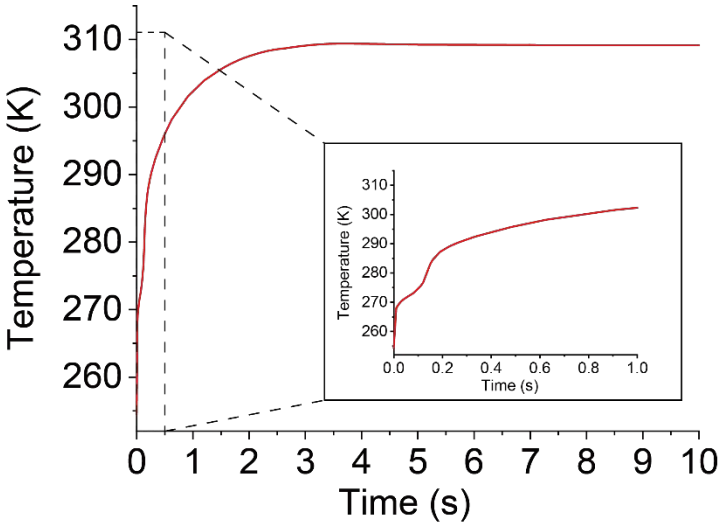


**Figure S4 (b)** Temporal evolution of the temperature at the top of ice in the model shown in Fig. S 4a.

**ESI 5. Calculated temperature distributions in hemispherical particle and bulk ice.**

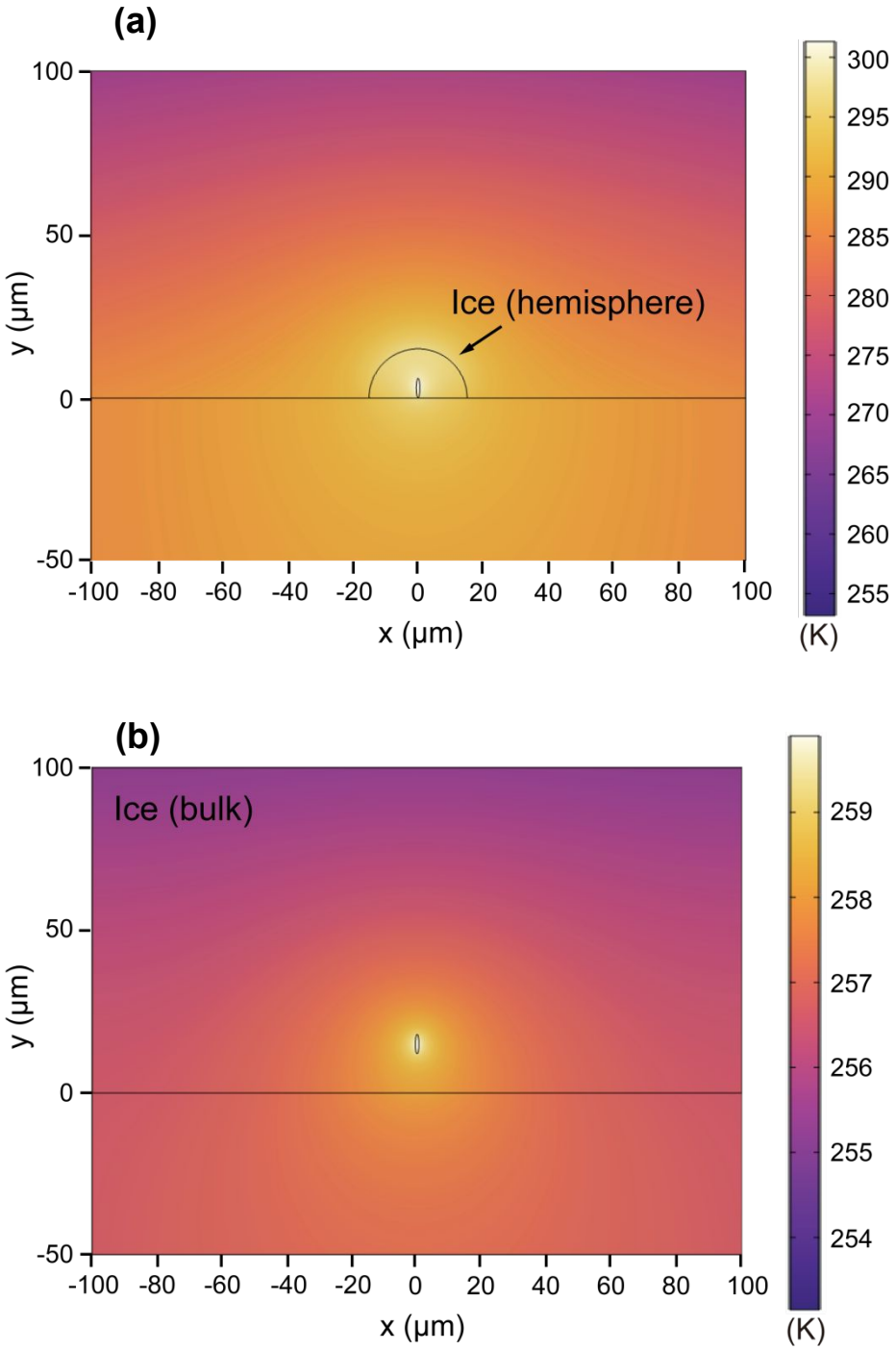


**Figure S5** (a) Temperature distribution for d=30 μm hemispherical ice particle supported on a substrate, (b) Temperature distribution in 200×200×200 $\mu m^3$ cubic ice that represents bulk ice. Max temperatures obtained are 301 K in a and 260 K in b.

**ESI 6. Observation of slow sublimation without melting of ice particle at low laser intensities.**

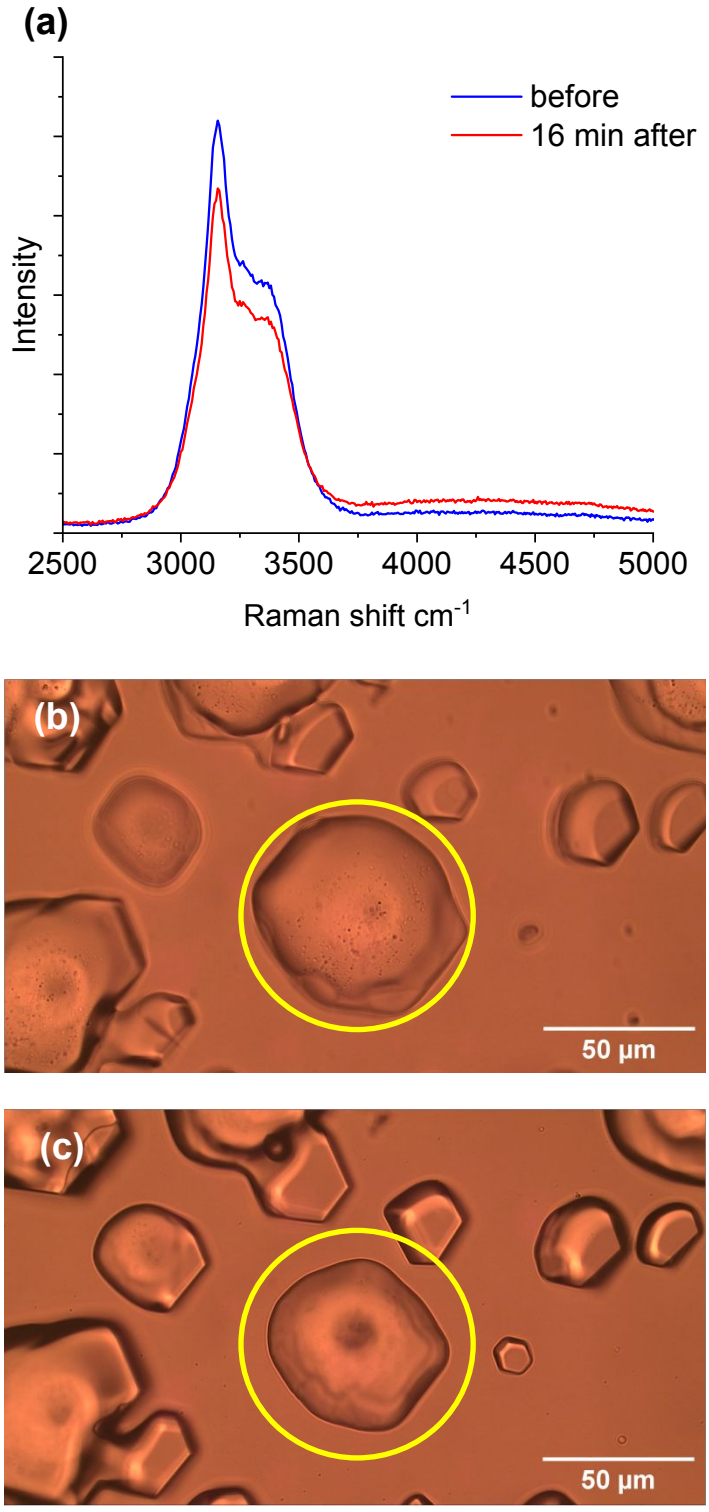


**Figure S** (a) Raman spectral change of ice before (b, ~70 μm) and after (c, ~50 μm) 1064-nm laser illumination with an intensity of 20 mW for 16 min (environmental temperature: −13°C.). Each spectrum was acquired after 10 s of exposure. Raman spectra were unchanged during the illumination that caused a gradual particle size reduction.

**ESI 7. Observation of evaporation from ice particle at high laser intensities.**

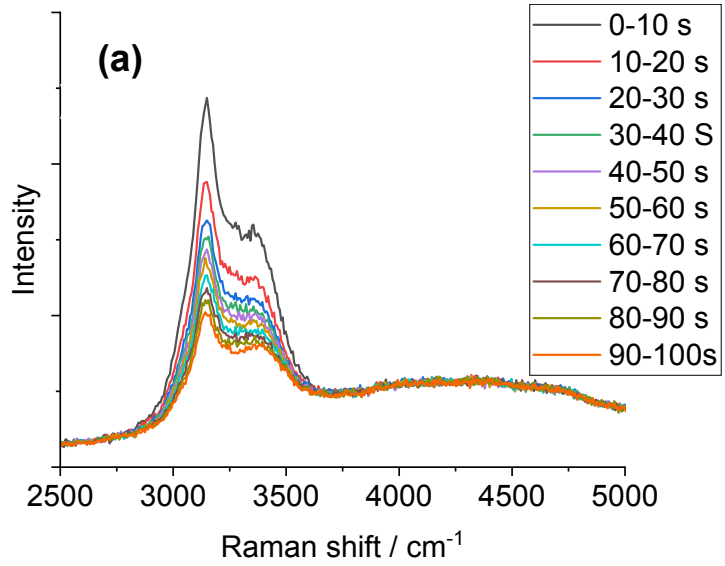


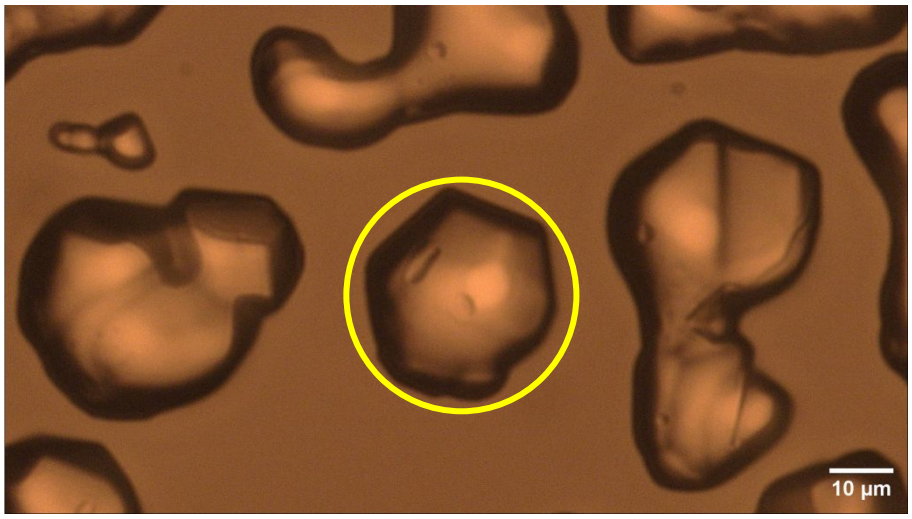


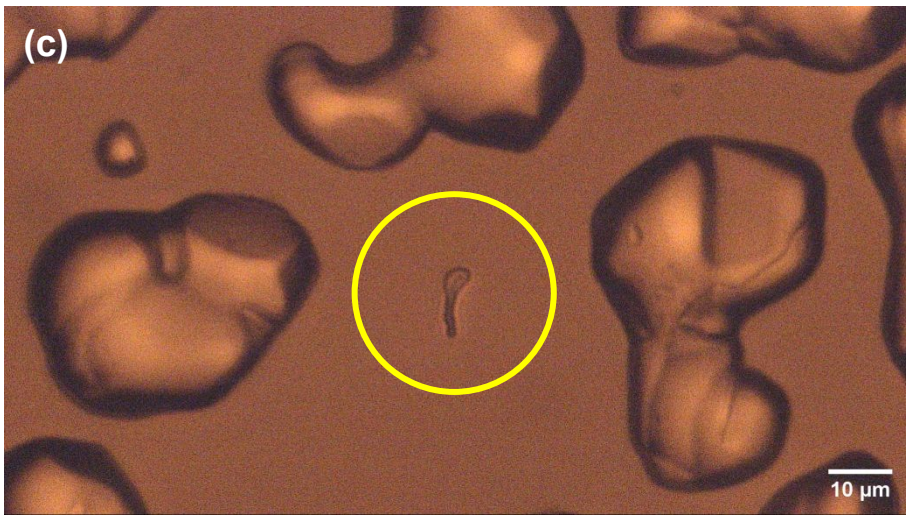


**Figure S** (a) In-situ Raman spectra of ice before (b, ~30 μm) and after (c) 1064-nm laser illumination with an intensity of 200 mW for 100 s (environmental temperature: −10°C.). Raman spectral shapes were unchanged during the illumination that caused a fast particle size reduction.

**ESI 8. Laser-power and particle diameter-dependent temperature distribution on water droplets.**

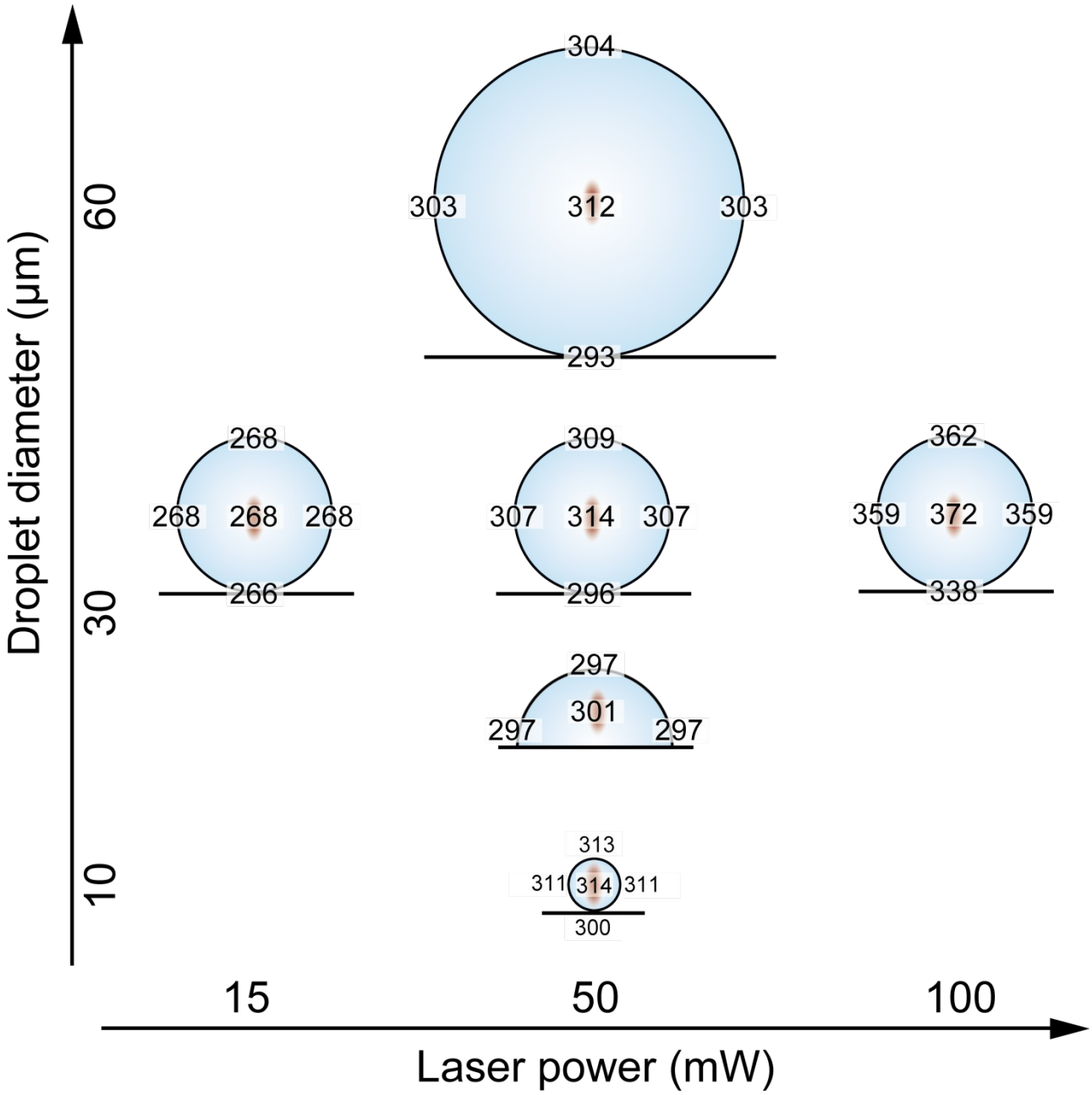


**Figure S** Calculated temperature (K) distributions using COMSOL for droplets with various diameters under laser illumination. Initial condition is that ice particles are supported on a glass substrate at 253 K (−20°C).

**ESI 9. Raman spectral changes observed for bulk ice on photothermal heating of gold nanoaggregates[13,14].**

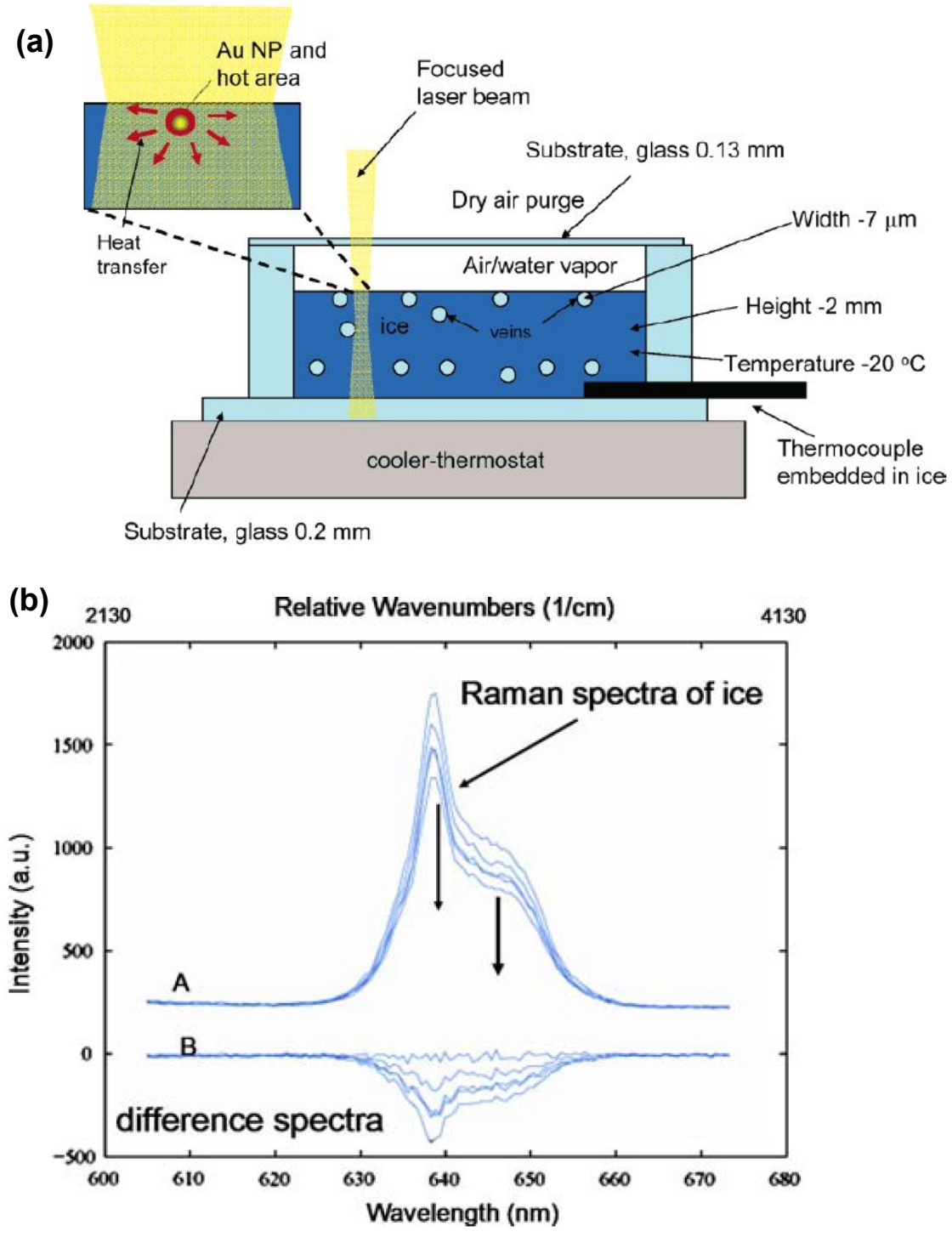


**Fig S6** (a) Experimental well (3-mm in diameter and 3-mm deep) that contains ice embedded AuNPs, showing 50-nm Au NP excited with a focused laser beam and heat transfer to the ice matrix.

(b) Experimental Raman spectral evolution of ice on 532-nm laser irradiation.

**References**


1. J. Trägårdh, K. Macrae, C. Travis, R. Amor, G. Norris, S. H. Wilson, G.-L. Oppo, G. McConnell, *J. Microscopy*, 2015, **259**, 66–73.
2. https://www.comsol.com/blogs/using-the-material-libraries-in-comsol-multiphysics/
3. J. G. Erwin, F. G. Peterman,; Schmidt, C.F. Laser-Induced Heating in Optical Traps. *Biophys. J.* 2003, 84, 1308–1316.
4. S. Ito, T. Sugiyama, N. Toitani, G. Katayama, H. Miyasaka, Application of Fluorescence Correlation Spectroscopy to the Measurement of Local Temperature in Solutions under Optical Trapping Condition. *J. Phys. Chem.* B 2007, **111**, 2365-2371
5. https://www.comsol.com/heat-transfer-module
6. https://www.comsol.jp/model/phase-change-474
7. H. H. Richardson, Z. N. Hickman, A. O. Govorov, A. C. Thomas, W. Zhang, M. E. Kordesch, Thermooptical properties of gold nanoparticles embedded in ice: characterization of heat generation and melting. *Nano Lett*. 2006, **6**, 783–788.